Edinburgh Research Explorer

Transient and steady state analysis of drill cuttings transport phenomena under turbulent conditions

Transient and Steady State Analysis of Drill Cuttings Transport Phenomena under Turbulent Conditions

Emmanuel I. Epelle and Dimitrios I. Gerogiorgis*

Institute for Materials and Processes (IMP), School of Engineering, University of Edinburgh, The King's Buildings, Edinburgh, EH9 3FB, United Kingdom

Corresponding author: D.Gerogiorgis@ed.ac.uk (+44 131 6517072)

ABSTRACT

Understanding the intricacies of multiphase flows is paramount to any drilling operation, and this has been under continuing and intensive development for the past decades. A major complexity associated with this operation is the uncertainty in the transport phenomena of generated cuttings as drilling progresses under different attainable configurations and fluid rheological conditions. Increased transport efficiency of drill cuttings in most drilling operations is usually characterised by an increased mud circulation velocity; this creates complex turbulent interactions between the solid and liquid phases. The study of the dispersion of these cuttings, in relation to their axial, tangential and slip velocity profiles in the annulus is carefully investigated in this work under steady and transient conditions. Computational Fluid Dynamics models (Eulerian-Eulerian, Lagrangian-Eulerian/Discrete Element Method) are utilised for this purpose. The implementation of the Eulerian-Eulerian model provides a macroscopic description of the distribution of fundamental flow properties such as pressure, volume fractions and velocities of each phase. Furthermore, a direct description of the particulate flow, inherent transient motion, interparticle and particle-wall collisions are obtained with the particle tracking functionality of the Lagrangian-Eulerian/DEM technique. The results obtained using the Eulerian-Eulerian model reveal that particle slip velocities are lowest at the central regions of the annulus with the effect of asymmetry due to inner pipe rotation being more pronounced along the longitudinal plane. Particle diameter has tremendous effects on the alteration of turbulence properties of the continuous phase with very distinct velocity profiles. Cuttings trajectory analysis show some extra phenomena which have been physically observed in available experimental studies; one of which is the occurrence of ejections of coherent structures at the walls of the flow domain. The difficulty of carrying out transient and steady state experimental measurements of particle velocities is an area where CFD shows great potential. The few available data in literature are well predicted with errors less than 11%. Similarly, fluid axial and tangential velocity predictions carried out, yield reasonably accurate results, thus further validating the CFD approach employed in this work.

1.

1. Introduction

Two challenging issues that persist in the relatively mature field of Computational Fluid dynamics are turbulence and multiphase flows (Brennen, 2005). There are gaps in the understanding of the physical phenomena, thus leading to difficulties in the development and successful implementation of modelling techniques. Obviously, the ability to predict the particle-fluid flow behaviour during drilling operations is central to the effectiveness and efficiency of a drilling program. Flows considered here usually have some level of phase or component segregation at a scale well above the molecular level. A peculiar and critical problem in understanding the behaviour of turbulent flows containing particles is the prediction of the distribution of the dispersed phase and its rate of impaction on boundaries (Roco, 1993). Furthermore, the complexities and consequences of unsteady relative motion, in which the particle, the fluid or both are accelerating due to hole inclination requires considerable attention.

The study of particle dispersion and precise identification of important physical mechanisms involved during turbulent flow conditions require highly coordinated and intensive experimental studies. The processes of monitoring and controlling dispersion are interactive, transient and require extensive 3D and time-dependent global visualisation techniques, thus complicating experimental methods (Roco, 1993; Crowe et al. 2011). Additional complexity ensues with the need to determine the two-way coupling effects between the particles and fluid (coupling of mass, momentum and energy transfer). Although experiments of such kind hold considerable promise for revealing new phenomena, the considerations are indicative of the fact that these investigations would be rather too complex. Many researchers have demonstrated via experiments that cuttings transport is affected by drilling variables such as pipe rotation, hole inclination and many other factors (Iyoho et al. 1986; Capo et al. 2004; Chen et al. 2007; Duan et al. 2006; Duan et al. 2010; Han et al. 2010; Osgouei, 2010; Ozbayoglu et al. 2010; Xu et al. 2013). It is worth mentioning that a majority these works have analysed cuttings transport phenomena as a function of the cuttings concentration and pressure drop which are relatively easy to physically measure. However, only a few studies exist in literature that analyse the velocities of particles, due to the difficulties earlier mentioned. The Positron Emission Particle Tracking (PEPT) technique has been implemented in analysing particle transport velocity profiles with a non-Newtonian fluid under laminar conditions in a pipe (Barigou, 2004; Eesa and Barigou 2008; Eesa and Barigou 2009). Similarly, cuttings slip velocity has been determined by Garcia-Hernandez et al. (2007) through optical measurements of specially marked cuttings in a transparent annulus. The effects of flow rate, pipe rotation and loop inclination were investigated using a moving camera system with water and a polymer-based drilling fluid. However, CFD techniques possess great potential for the elucidation of these complexities.
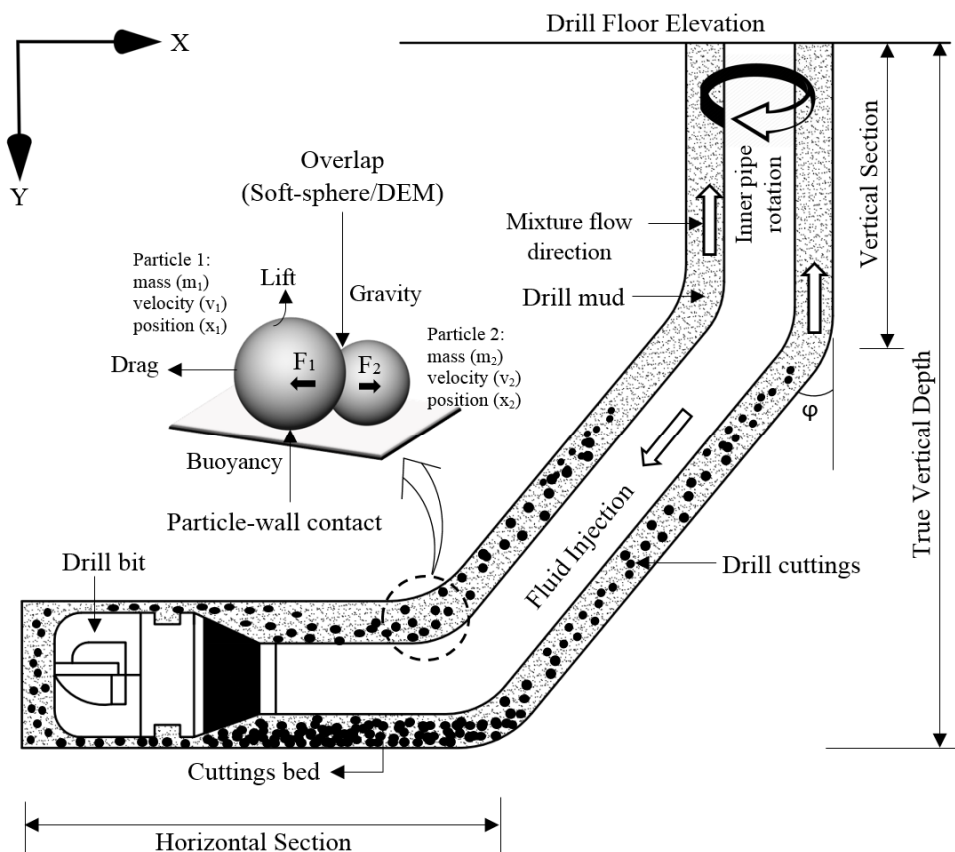

Fig 1. Drilling operation and wellbore cleaning with fundamental concepts of the adopted CFD modelling methods.

Although, at this stage, comprehensive constitutive relationships for modelling have not been fully established, several approaches which have proved useful are available for predicting solid-liquid behaviour (Fan and Zhu, 2005), particularly for drilling applications. Among them are the Eulerian continuum approach, Lagrangian trajectory approach and the kinetic theory modelling (with similar concepts in the DEM technique) for interparticle collisions. The Eulerian continuum approach, based on a continuum assumption of phases, provides a field description of the dynamic behaviours of each phase. The Lagrangian trajectory approach, from the study of motions of individual particles, is capable of providing historical trajectories of the particles (Subramaniam, 2013). The kinetic theory modelling for interparticle collisions, extended from the kinetic theory of gases, is applicable to dense particulate systems where the transport of the particle phase is dominated by inter-particle collisions (Fan and Zhu, 2005). However, the most common method of analysis of cuttings transport phenomena is the RANS equations implemented within the Eulerian framework (Bilgesu et al. 2002; Bilgesu et al. 2007; Mishra, 2007; Sorgun, 2010; Ofei et al. 2014; Rooki et al. 2014; Rooki et al. 2015; Heydari et al. 2017). These investigations majorly evaluate the impact of several drilling variables on the efficiency of cuttings transport with respect to the cuttings volume fraction.

On the other hand, the Discrete Phase Model has been implemented by Pereira et al. (2010) for the analysis of the flow phenomena of cuttings in an annulus with special consideration given to particle trajectory as a function of drill pipe rotation. Wang et al. (2009) in their study on the transport process of cuttings in extended reach wells under the influence of drill pipe rotation, discovered circumferential/quasi-spiral solid-liquid flow coupled with the principal axial flow in the annular space. Yilmaz (2012) investigated cuttings bed height and particle trajectories using the one-way Lagrangian-Eulerian coupling scheme and predicted experimentally obtained data with good accuracy. Demiralp (2014) examined the effects of drill pipe whirling motion on cuttings transport performance in eccentric horizontal annuli. In his work, the two-way coupling of the particle-fluid interactions using the Discrete Element Method (DEM) was implemented. A corresponding increase in pressure with an increase in the whirling speed was observed. The effect of particle shape on the cuttings transportation mechanism in well drilling has been thoroughly investigated by Behzad et al. (2015) using the Discrete Element Method (DEM). They were able to reasonably predict experimental data and concluded that particle shape plays a major role in the fluid-solid interaction. Various numerical simulations have been carried out by Bertrand et al. (2005) using the DEM model for the prediction of granular behaviour. They emphasized that the computational time required for the implementation of the DEM technique could be very high, although its ability to capture key flow phenomena could be remarkable.

A previous study of ours (Epelle and Gerogiorgis, 2017) analysed the impact several drilling variables on majorly the cuttings concentration and pressure drop with more attention on the impact of changing hole eccentricity. This was entirely carried out under steady state conditions while considering a laminar flow regime using the Eulerian-Eulerian model. No quantitative detailed analysis was conducted for the spatial velocity variation under turbulent conditions; moreover, such kind of analysis for drilling applications is rare in literature to the best of our knowledge. Furthermore, cuttings of single uniform size distribution (3mm diameter) were used in the earlier paper, with no consideration given to flow peculiarities when smaller or larger cuttings are transported. This paper seeks to address this gap by evaluating the interdependencies between cuttings trajectory profiles and several drilling variables of interest. Special emphasis is laid on the slip, tangential and axial velocities and the cuttings diameter as major determinants of transport efficiency under turbulent flow conditions. CFD simulations are performed to solve the governing flow equations in ANSYS Fluent 17.1 using the power law model to describe the non-Newtonian drilling fluid rheology and the k-ω model for evaluating the turbulent interactions between both phases. The theoretical and mathematical formulation of the implemented models is summarized next, followed by a mesh independence study. The results of the impact of drilling variables is discussed subsequently and conclusions derived.

2. Methodology

2.1. CFD Modelling

Both the Eulerian and Lagrangian approaches are adopted for the analysis of cuttings transport phenomena in this study. The Eulerian-Eulerian (EE) model in which particles act like a continuum phase is adopted for steady state modelling. This approach is basically an extension of the mathematical formulation of the fluid dynamics for a single phase to a multiphase system (Fan and Zhu, 2005). Phase interactions are thus expressed in a continuous form and the transport and turbulent properties of each phase determined. Appropriate closure models are implemented in order to recapture important particle phenomena lost due to the inherent averaging property of this model (Liu, 2014). Interphase drag, shear, bulk and granular viscosities are the major phenomena which are necessary for complete closure and solvability of the governing flow equations.

The principal motivation for applying the Lagrangian approach is that the physics of flow emerges in a more natural way (Roco, 1993) thus providing further insight into the transport phenomena of cuttings. In essence, a statistical description of the dispersed phase is coupled with an Eulerian statistical representation of the carrier fluid phase (Subramaniam, 2013). In this approach, an understanding of the time dependency of turbulent diffusion is substituted for the determination of the spatial variation of a diffusion coefficient used in the Eulerian model (Binder and Haratty, 1991). Another element of superiority of the LE model is seen in the way gravitational settling in horizontal flows (which causes asymmetries in particle concentration profiles) is handled. The EE model usually takes this into account by assuming the settling velocities of the particles to be equal to their terminal values in the constitutive/closure equations. This could be slightly inaccurate because the particles might not have been in the field long enough to attain free fall; the use of an equation (LE) for the particle trajectory in the description of diffusion from a small wall source takes this into account (Roco, 1993).

Discrete Phase Model (DPM) and the Discrete Element Method (DEM) are concurrently implemented in the Lagrangian-Eulerian (LE) approach in ANSYS Fluent. By using both methods, the limitation of the DPM model in handling dilute flows (with particle volume fractions less than 12%) is circumvented (ANSYS Fluent, 2017). Historic tracking of particles using the DEM method allows interparticle and particle-wall collisions that dominate dense flows to be accurately captured (Subramaniam, 2013). At higher particle concentrations, a whole spectrum of complications arises in which the motions of the dispersed and continuous phase are simultaneously affected; thus, necessitating a 2-way coupling solution (Brennen, 2005). In a bid to enhance convergence of the 2-way coupling scheme in Fluent, the particle tracking time step was set to the same value as that of the fluid (10^{-4}), hence yielding good particle response times in relation to the time associated with the turbulent motion of the fluid (Stokes number).

2.2. Choice of turbulence model

The problem of turbulence and particle interactions as it relates to drilling operations has three major aspects: the dispersion of particles due to turbulence of the carrier fluid, particle segregation due to complex unsteady motions (non-uniform particle spatial distribution) and the modulation of the turbulence due to the presence and motion of particles (Hetsroni, 1989). It is possible to visualise that turbulence may be enhanced by the wakes and other structural disturbances that the motion of the particles instigate or dampened by the apparent bulk viscosity that the presence of particles introduce (Brennen, 2005). In order that these concepts are accurately accounted for, appropriate wall treatment is essential. The Standard k-ω model was considered the most suitable due to its superior performance for wall bounded/boundary layer flows, transitional flow modelling capability and its adaptability to flows involving rotation. Despite the robustness of the k-ε models, the method of handling near wall flows via wall functions made them less suitable compared to the Standard k-ω model. Essentially, these wall functions neglect the flow field in the buffer region and assume an analytical solution in the viscous layer; this is not necessary in the k-ω model because they are valid all the way to the wall provided the mesh used is sufficiently fine (ANSYS Fluent, 2017).
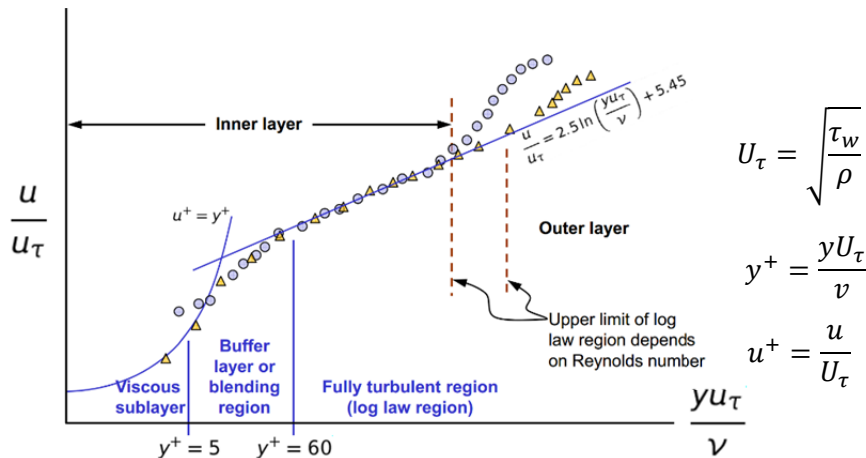
Fig. 2. The law of the all and near-wall treatments (ANSYS Fluent, 2017)

2.3. Simulation strategy

The Reynolds Averaged Navier Stokes (RANS) equations (continuity, momentum and transport equations) are numerically solved in a discretised domain using the finite-volume formulation. In the steady state turbulent Eulerian-Eulerian approach, pressure-velocity coupling was effected using the phase coupled Semi-Implicit Method for Pressure-Linked Equations (SIMPLE) scheme. The effect of numerical diffusion on the solution accuracy is mitigated by employing second order accurate solution schemes (Second Order Upwind) for the momentum and turbulent

parameters. The volume fraction is spatially discretised using the Quadratic Upstream Interpolation for Convective Kinematics (QUICK) method. Iterative convergence is achieved with at least three orders of magnitude decrease in the normalised residuals for all equations solved. Also, under-relaxation factors were appropriately tuned to avoid unphysical oscillations in the calculations, thus ensuring stable convergence. A velocity inlet boundary condition (Table 1) is specified alongside a pressure outlet at atmospheric pressure. The nature of the flow condition being studied (fully-developed internal annular flow), warranted the specification of the Turbulent Intensity and Hydraulic Diameter as the turbulent mixture boundary condition. These were estimated to be 4.5% and 0.07 m respectively. The wall boundaries were treated according the conventional fluid mechanics no-slip condition; in which particles in contact with the wall cannot move relative to wall. However, the occurrence of slip at the walls was rather inevitable as shown in the results section. Furthermore, the Lun et al. (1984), Gidaspow, (1994) and Saffman-Mei (1965) models were the main closure models implemented to account for the viscosity, drag and lift forces of the granular phase respectively.
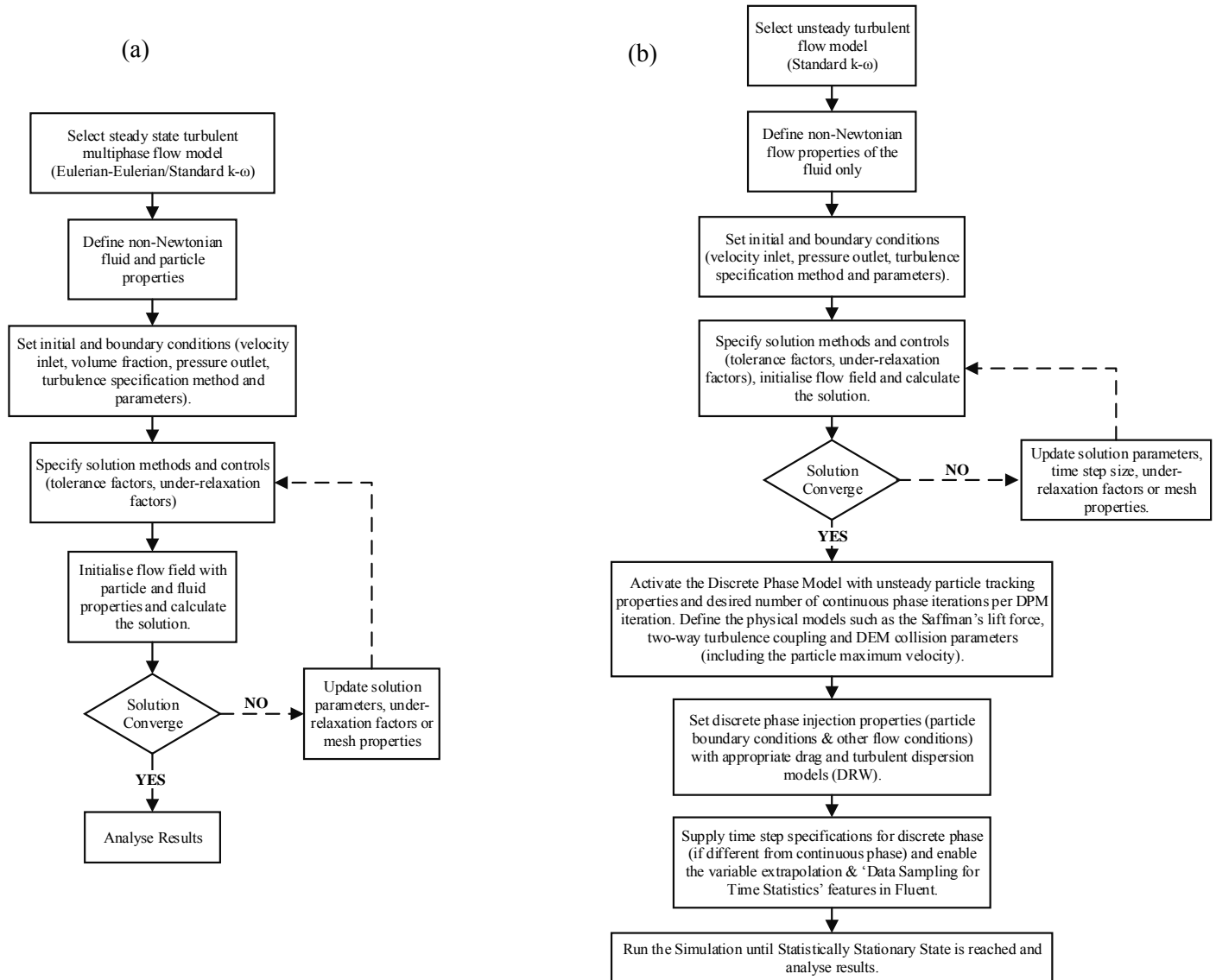

Fig. 3. Simulation procedure for the (a) Eulerian-Eulerian model (b) Lagrangian-Eulerian model

The general procedure with the LE approach is usually to solve the RANS equations of the continuous phase first without particle injections for convergence before introducing the particles. Very similar specifications to the EE model were adopted in the unsteady state turbulent LE approach; however, the transient flow modelling and the treatment of the discrete phase are extra complications that required additional specifications. Firstly, the mean flow residence time (ratio of characteristic length to mean flow velocity) in the flow domain was determined to be 1 second. The simulation was run for a few mean flow residence times until Statistically Stationary State (SSS) was achieved. The 'Data Sampling for Time Statistics' tool in Fluent was employed for post processing the mean (time averaged) values of the velocities and volume fractions. Good convergence at each time step of the transient calculations was attained by implementing the 'Extrapolate Variables' option in Fluent (This enables prediction of the solution variables of the subsequent time step using a Taylor series expansion).

5

Johnson and Jackson (1987) showed that the manner of entry of granular material into an annulus affects the transport phenomena down the annulus. They discovered that the flow behaviour far from entry was affected by the inlet conditions at high flow rates as opposed to low flowrates. Turbulent conditions used in this study thus required a careful selection of the boundary conditions. Particles of uniform diameter were injected at an inlet fraction of 20% and a 50 ft.hr^{-1} ROP (Eq. 22). The method proposed by Larsen et al. (1997) was used for the determination of the inlet velocity (Eq. 22-23). The relatively high (>12%) entry particle volume fraction implies that stochastically tracked particle trajectories would be affected by interparticle collision, particle-wall collisions and particle–fluid interactions; hence the DEM method (soft sphere approach in which particles slightly overlap) and 2-way turbulence coupling is implemented in Fluent. In order to effect this, the number of discrete phase iterations per continuous iterations is set to a sufficiently large value to allow the continuous phase to absorb the change in momentum through the source terms of the discrete phase. The Discrete Random Walk Model is also included in the simulation setup to incorporate the effect of turbulence on the fluctuations in particle velocities due to eddy formation. Fig. 3 summarises the simulation procedures implemented for the steady and transient studies respectively.

2.4. Closure models used to describe particle behaviour in the Eulerian-Eulerian model

2.4.1. Total solids viscosity

The total viscosity of the solid phase is calculated as:

$$\mu_p = \mu_{p,col} + \mu_{p,kin} + \mu_{p,fr} \tag{1}$$

2.4.2. Collisional viscosity

The collisional component of the shear viscosity proposed by Gidaspow (1994) is modelled as:

$$\mu_{p,col} = \frac{4}{5}\alpha_p\rho_p d_p g_{0,SS}(1 + e_{SS})\left[\frac{\Theta_p}{\pi}\right]^{1/2}\alpha_p \tag{2}$$

2.4.3. Kinetic viscosity

According to Gidaspow (1994):

$$\mu_{p,kin} = \frac{10\rho_p d_p\sqrt{\Theta_p\pi}}{96\alpha_p(1 + e_{SS})g_{0,SS}}\left[1 + \frac{4}{5}g_{0,SS}\alpha_p(1 + e_{SS})\right]^2\alpha_p \tag{3}$$

2.4.4. Bulk viscosity

The bulk viscosity accounts for the resistance the particles possess against compression and expansion during flow. Lun et al. (1984) described this effect as:

$$\lambda_p = \frac{4}{3}\alpha_p^2\rho_p d_p g_{0,SS}(1 + e_{SS})\left[\frac{\Theta_p}{\pi}\right]^{1/2} \tag{4}$$

2.4.5. Frictional viscosity

The frictional component of the total solids viscosity is applicable to dense flows at low shear, in which the solids volume fraction approaches the packing limit and is calculated using the model proposed by Schaeffer (1987).

$$\mu_{p,fr} = \frac{p_p \sin \phi}{2\sqrt{I_{2D}}} \tag{5}$$

2.4.6. Particle drag model

The model proposed by Gidaspow (1994) combines the Wen and Yu (1966) model and the Ergun equation for accurate solutions. The Gidaspow interphase drag model can also be used for large volume fractions, especially at high ROPs. This flexibility is not offered by the Wen and Yu drag model.

When $\alpha_l > 0.8$, the fluid-particle exchange coefficient, K_{pf}, is calculated as:

$$K_{pf} = \frac{3}{4} C_D \frac{\alpha_p \alpha_f \rho_f |\vec{v}_p - \vec{v}_f|}{d_p} \alpha_l^{-2.65} \tag{6}$$

where

$$C_D = \frac{24}{\alpha_l Re_s}[1 + 0.15(\alpha_f Re_s)^{0.687}] \tag{7}$$

When $\alpha_l \leq 0.8$,

$$K_{pf} = \frac{150\alpha_p(1 - \alpha_f)\mu_f}{\alpha_f d_p^2} + 1.75\frac{\alpha_p \rho_f |\vec{v}_p - \vec{v}_f|}{d_p} \tag{8}$$

2.4.7. Particle lift model

The Saffman-Mei lift force model was adopted in ANSYS-Fluent (Saffman, 1968; Mei and Klausner, 1994). Its applicability to spherical and slightly distorted particles make it more robust compared to the Moraga (1999) lift force model.

$$C_l = \frac{3}{2\pi\sqrt{Re_\omega}}C'_l \tag{9}$$

$$C'_l = 6.46 \; and \; 0 \leq Re_p \leq Re_\omega \leq 1 \tag{10}$$

Mei and Klausner (1994) extended the model to a higher range of particle Reynold numbers (Re_p). Hence, the Saffman-Mei model can be empirically represented as:

$$C_l = \frac{3}{2\pi\sqrt{Re_\omega}}C'_l \tag{11}$$

$$C'_l = \begin{cases} 6.46 \times f(Re_p, Re_\omega) & Re_p \leq 40 \\ 6.46 \times 0.0524(\tilde{\beta}Re_p)^{1/2} & 40 < Re_p < 100 \end{cases} \tag{12}$$

where

$$\tilde{\beta} = 0.5(Re_\omega/Re_{p)} \tag{13}$$

$$f(Re_p, Re_\omega) = (1 - 0.3314\tilde{\beta}^{0.5})e^{-0.1Re_p} + 0.3314\tilde{\beta}^{0.5} \tag{14}$$

$$Re_p = \frac{\rho_q |\vec{v}_f - \vec{v}_p|d_p}{\mu_f} \tag{15}$$

$$Re_\omega = \frac{\rho_q |\nabla \times \vec{v}_p|d_p^2}{\mu_f} \tag{16}$$

2.5. Equations of particle motion in the Lagrange-Eulerian model

ANSYS Fluent predicts particle trajectory of the discrete phase by integrating by integrating the force balance on the particle in the Lagrangian reference frame. This force balance can be described as:

$$\frac{d\vec{v}_p}{dt} = F_D(\vec{v}_f - \vec{v}_p) + \frac{\vec{g}(\rho_p - \rho_f)}{\rho_p} + \vec{F} \tag{17}$$

Where $\vec{F}$ is an additional force (consisting of virtual mass and pressure gradient forces, which are not important when the density of the fluid is much lower than the density of the particles), $F_D(\vec{v}_f - \vec{v}_p)$ is the drag force per unit mass, $\vec{u}$ is the fluid velocity, μ_f is the molecular viscosity of the fluid, ρ_f is the fluid density, ρ_p is the density of the particle, and d_p is the particle diameter. Re_s is the relative Reynolds number, defined as:

$$F_D = \frac{18\mu_f}{\rho_p d^2{}_p} \frac{C_D Re_s}{24} \tag{18}$$

$$Re_s \equiv \frac{\rho_f d_p |\vec{v}_p - \vec{v}_f|}{\mu_f} \tag{19}$$

When a moving reference frame is involved, the additional force term incorporates the forces on particles due to drill pipe rotation. For rotation about the z axis, the forces in Cartesian x and y coordinates can be written as:

$$\left(1 - \frac{\rho_f}{\rho_p}\right)\Omega^2 x + 2\Omega\left(v_{p,y} - \frac{\rho_f}{\rho_p} v_{f,y}\right) \tag{20}$$

Where $v_{p,y}$ and v_y are the particle and fluid velocities in the Cartesian y direction, Ω is the RPM, and

$$\left(1 - \frac{\rho_f}{\rho_p}\right)\Omega^2 y + 2\Omega\left(v_{p,x} - \frac{\rho_f}{\rho_p} v_{f,x}\right) \tag{21}$$

Where $v_{p,x}$ and $v_{f,x}$ are the particle and fluid velocities in the Cartesian x direction. Turbulent dispersion of particles in the fluid phase can be predicted using the stochastic tracking (random walk) model which includes the effect of instantaneous turbulent velocity fluctuations on the particle trajectories. Details of this method, the Discrete Element Method (DEM) for interparticle collisions and accompanying equations are presented in the ANSYS Fluent Theory Guide (Fluent 2017). Furthermore, in order to determine the appropriate entry conditions for the cuttings, Eq. (22 –24) were used.

$$\dot{m} = \frac{ROP \times \rho_p \times A_{annulus}}{\left[1 - \left(\frac{D_{pipe}}{D_{wb}}\right)^2\right]} \tag{22}$$

$$v_p = \frac{\dot{m}}{\rho_p \times A_{annulus} \times c_p}; \; where \; A_{annulus} = \frac{\pi}{4}(D^2{}_{wb} - D^2{}_{pipe}) \tag{23}$$

$$c_p = \frac{\text{Net volume occupied by particles}}{\text{Total volume of annulus}} \times 100 \tag{24}$$

2.6. Computing requirements

The computational time is significantly affected by the chosen turbulent model and the phase interaction mechanisms. Also, accurate evaluation of the dynamic character of the mobile liquid and particle phases in Lagrangian coordinates requires the implementation of stochastic trajectory models, in which thousands of trajectories are determined (Fan and Zhu, 2005). Enormous computing power is thus needed to carry out the numerous iterations necessary to obtain converged solutions for all phases. Conversely, the steady state Eulerian-Eulerian calculations, are to a great extent, computationally less intensive than the transient CFD/DEM method. Simulations were run for a period of approximately 30 days on the University's high performance computing facility (Eddie mark 3 – Scientific Linux 7 Operating System) with 16 cores (2.4GHz Intel®-Xenon® CPU processor) and 64GB of RAM.

2.7. Drilling fluid rheology and annular flow geometry

In both steady and transient state simulations, the adopted drilling fluid was a 0.8 wt.% aqueous CMC solution with power law parameters determined from the experimental and numerical investigations of Eesa and Barigou (2009). In order to comparatively evaluate the performance of the drilling mud of non-Newtonian rheology with a Newtonian carrier fluid, simulations are carried out using water. Fluid and solid properties used in this study are shown in Table 1.

Table 1. Simulation parameters

Geometry	Eulerian-Eulerian	Lagrangian-Eulerian
Drill pipe diameter (m)	0.10795	0.10795
Wellbore diameter (m)	0.17780	0.17780
Computational Length (m)	11	2
Particle properties (spherical)		
Cuttings diameter (mm)	1, 5,10	1, 5, 10
Cuttings density (kg.m^{-3})	2610	2610
Fluid properties		
Density (kg.m^{-3})	1000	1000
Consistency index, K (Pa.s^n) = τ/γ^n	0.16	0.16
Flow behaviour index (n)	0.81	0.81
Drilling variables		
ROP (ft.hr^{-1})	50, 100	50, 100
Fluid circulation velocity (m.s^{-1})	1.5	2
Flow regime	Steady state turbulent	Unsteady state turbulent
Drill pipe rotation (RPM)	100, 400	100, 400
Hole eccentricities (e)	0, 0.6	0.6
Hole inclination from vertical (degrees)	0, 45, 90	0, 45, 90

The flow geometry considered comprises of two walls. The stationary outer wall represents the wellbore while the inner wall was modelled with a rotation effect in order to simulate the rotation of the drillpipe. The magnitudes of this rotary motion were 100 RPM and 400 RPM respectively. On the other hand, translational drillpipe movements of the drillpipe were considered negligible and ignored. Although some researchers have developed empirical correlations for the entrance length prediction of fully developed turbulent flows (Nikuradse, 1966; Lien et al. 2004; Cengel et al. 2005), test simulations were carried out to monitor the development of the velocity boundary layer before deciding on the length of the flow main. As seen in Table 1, the length of 2m was used for the CFD/DEM simulation and is considerably lower than that adopted for the steady state simulation. This is obviously due to high computational burden of transient multiphase flow simulations. Also, concentric and eccentric flow configurations were separately analysed for their flow peculiarities. Tables 2 and 3 summarise the geometric properties of both configurations (Fig. 4 and 5).
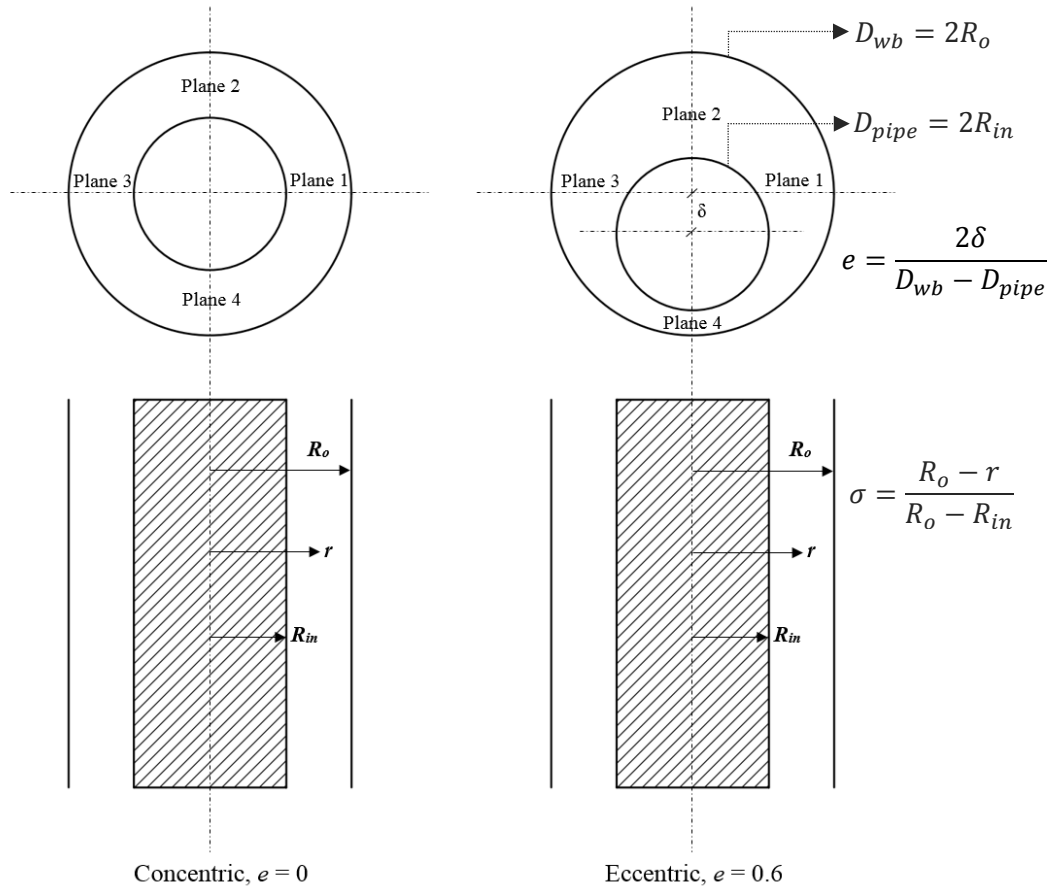
Fig. 4. Geometric set-up with line-planes used for the analysis of cuttings transport phenomena

2.8. Mesh independence study

Sufficiently fine hexahedral structural meshes were implemented for the concentric and eccentric configurations comprising of 2.5×10^6 elements (11m computational length) for the Eulerian-Eulerian model and 3.3×10^5 elements (2m computational length) for the Lagrangian-Eulerian model. For the concentric flow configuration, 60 edge divisions and 30 radial divisions were adopted whereas 70 edge divisions and 20 radial divisions were implemented in the eccentric case, thus yielding good mesh resolution capable of capturing near wall effects. These corresponded to a uniform first layer thickness of 1.2 mm in the concentric domain, while 0.5 mm and 1.9 mm were the minimum and maximum values in the eccentric domain. It was thus necessary to estimate the wall-adjacent cell centroid/dimensionless wall distance (y^+) before generating the mesh. This dimensionless quantity majorly ranged between 15 and 17 depending on the wall shear stress, and skin friction coefficients computed for the different flow conditions studied. While the CFD/RANS/DEM community continues to seek wall treatments methods that are insensitive to y^+ values as the mesh is refined, the k-ω eddy viscosity model was deemed the most appropriate for our study considering its ability to handle wall treatment without the use damping wall functions. Mesh qualities (orthogonality, skewness and aspect ratio) reported in Tables 2 and 3 further illustrate the credibility of the adopted meshing technique.

Solutions of velocity profiles, volume fractions and pressure drop are presented over a range of significantly different grid resolutions in order to demonstrate grid-independent/gird-convergent results. The mesh independence study was carried out using different total face divisions (number of edge division × number of radial divisions) while retaining the number of axial divisions. The simulation set up consisted of a horizontal annulus with 100 RPM inner pipe rotation and only profiles along plane 4 (See Fig. 6) are shown.

Table 2. Computational mesh properties of the concentric flow domain

Edge Divisions	Radial Divisions	y (mm)	Total Face Divisions	No. of Elements	No. of Nodes	Min. Orthogonality	Max. Skewness	Max. AR
50	10	3.49	500	613000	674850	0.9982	0.0400	3.14
50	20	1.75	1000	1226000	1288350	0.9981	0.0400	6.34
60	20	1.75	1200	1765200	1854720	0.9987	0.0333	5.28
70	20	1.75	1400	2402400	2523990	0.9990	0.0286	4.52
60	*30*	*1.16*	*1800*	*2647800*	*2737920*	*0.9986*	*0.0333*	*7.95*
70	30	1.16	2100	3603600	3725890	0.9990	0.0286	6.81

Table 3. Computational mesh properties of the eccentric flow domain

Edge Divisions	Radial Divisions	Min. y (mm)	Max. y (mm)	Total Face Divisions	No. of Elements	No. of Nodes	Min. Ortho.	Max. Skewness	Max. AR
50	10	5.59	1.40	500	637500	2742882	0.7787	0.4381	6.62
50	20	2.79	0.70	1000	1275000	5294412	0.7506	0.4381	13.31
60	20	2.79	0.70	1200	1750800	7269540	0.9631	0.1761	11.6
70	*20*	*2.79*	*0.70*	*1400*	*2453760*	*10187506*	*0.8297*	*0.3640*	*10.07*
60	30	1.86	0.47	1800	2626200	10772940	0.9597	0.1761	17.43
70	30	1.86	0.47	2100	3680640	15097156	0.8047	0.3640	15.12

Maximum first layer thickness

Uniform first layer thickness   Minimum first layer thickness
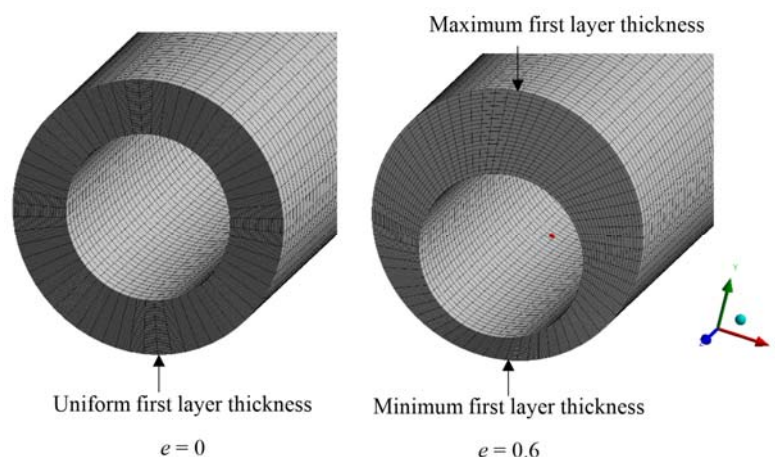
$e = 0$ $e = 0.6$

Fig. 5. Computation mesh for the concentric and eccentric flow configurations.

2.9. CFD model validation

As pointed out earlier, comprehensive measurements of the particle velocity profiles in solid–liquid flows are very scarce due to the inherent difficulty of performing such measurements with the available techniques. However, (Barigou et al. 2003 Eesa and Barigou, 2009) have carried out extensive experiments using the PEPT technique to determine the trajectories and velocity profiles of coarse solid particles flowing in non-Newtonian CMC carrier fluids. These unique experimental results are used to assess the accuracy of the numerical CFD simulations. Furthermore, the work of Garcia-Hernandez et al. (2007) provide some experimental measurements of cuttings lag velocity in an annulus which is also used for validation purposes. It is important to bear in mind that the data provided in these studies do not consider the tangential velocities of the phases that ensue as a result of the inner pipe rotation (Table 4). Hence, experimental results of (Nouri and Whitelaw, 1997; Escudier et al. 2002) whose studies take this into account, although with the turbulent flow of the carrier fluid alone, are useful for the validation process. Fig 6 shows good CFD predictions of the axial and tangential velocities of both phases using the Eulerian-Eulerian model with mean absolute errors less than 11%; thus illustrating the capability of CFD simulations to replicate physical flow phenomena encountered during drilling.
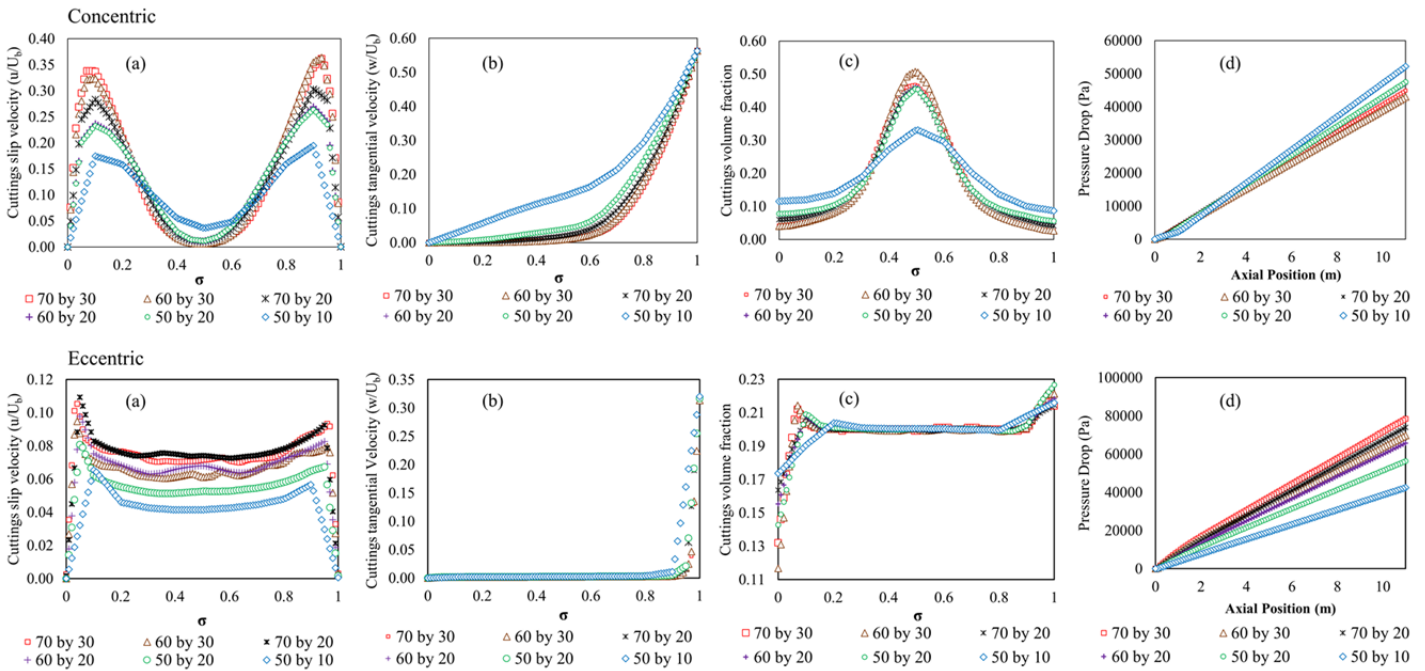

Fig. 6. Mesh independence study for concentric and eccentric flow domains

Table 4. Experimental data summary used for model validation

	Nouri & Whitelaw (1994)	Nouri & Whitelaw (1997)	Escudier et al. (202)	Garcia Hernandez et al. (2007)	Eesa & Barigou (2009)
Flow Geometry					
Drill pipe diameter (m)	0.0200	0.0200	0.0508	0.1143	-

Hole diameter (m)	0.0403	0.0403	0.1004`	0.2032	0.045
Computational Length (m)	2.32	2.32	5.775	30.48	0.6
Particle Properties					
Cuttings density (kg.m^{-3})	-	-	-	2610	1020
Cuttings diameter (m)	-	-	-	0.004	0.007
Fluid Properties					
Fluid type	0.2% CMC	0.2% CMC	0.1% (XG+CMC)	Water	0.8% CMC
Density (kg.m^{-3})	1000	1000	1100	998.5	1000
Consistency index, K (Pa.s^n)	0.044	0.044	1.305 (Cross)	0.001	0.81
Flow behaviour index (n)	0.75	0.75	0.509 (Cross)	1.0	0.16
Drilling variables					
ROP (ft.hr^{-1})	-	-	-	30	-
Fluid circulation velocity (m.s^{-1})	2.78	2.72	0.203	1.1 – 1.5	0.125
Flow regime	Steady state turbulent	Steady state turbulent	Steady state laminar	Steady state laminar	Steady state laminar
Drill pipe rotation (RPM)	300	300	50	0	-
Hole eccentricities (e)	0	0.5	0	0.8	-
Hole inclination from vertical (^{o})	0	0	90	90	90

Fig. 6. CFD model validation against experimental data

3. Results and Discussion

3.1. Analysis of velocity profiles in a concentric annulus using the Eulerian-Eulerian Model

The impact of drill pipe rotation, inclination angle, particle diameter and fluid rheology on the velocity profiles (axial, slip and tangential), volume fraction and pressure drop are presented and carefully examined in a concentric annulus. The presented profiles which give some insight into the flow phenomena, were generated from regions of fully developed flow in the annulus. All velocities are normalised by the bulk velocity (U_b) and the spatial variation of flow properties is determined as a function of the dimensionless annular space (σ).

3.1.1. Effect of drill pipe rotation

Fig. 7 shows a uniform magnitude in cuttings axial velocity across all planes with the highest values at the central annular regions. As observed in Fig. 7a-d, there is a slight degree of asymmetry in the axial velocity profiles with an increase in drill pipe rotation; this is more noticeable on planes 2 and 3. The profiles of axial velocity mostly overlap in all the planes and are relatively insensitive to the rotation effect. The slip velocity profiles exhibit a spike at the near wall regions and a minimum at the centre of the annulus in all plane sections considered, thus explaining the spatial variation in flow resistance demonstrated by the solid phase relative to the fluid. At the bottom of the annulus (Plane 4), the effect of pipe rotation is more pronounced. The impact of gravity in the inclined annulus is bound to increase the slip of the solid phase; however, an increased rotation effect tends to reduce the slip velocity (and eventual phase segregation), thus improving the efficiency of the transport process. The tangential velocity profile shows a sharp increase with the particles' position in the annulus approaching the rotating drill pipe. Obviously, this effect is higher with a rotation of 400 RPM compared to 100 RPM (Fig. 7i-l). It is possible to visualise the lifting effect rotation has on the particles, which is better explained by observing the volume fraction profiles (Fig. 7m-p). Compared to the slight spreading of particles observed at 100 RPM, the volume fraction is seen to have a slender peak at the centre position of the annulus at 400 RPM. This illustrates that more particles tend to travel in the centre region of the annulus with increased rotation (due to particle lifting). The volume fraction profiles illustrated in planes 3 and 4 reveal that pipe rotation effects are stronger along the longitudinal section of the annulus. Furthermore, the inclined configuration of the annulus implies the top part of the annulus and the lower part of the drill pipe are almost void of cuttings; this is shown in planes 2 and 4 (Fig. 7n and 7p) respectively.
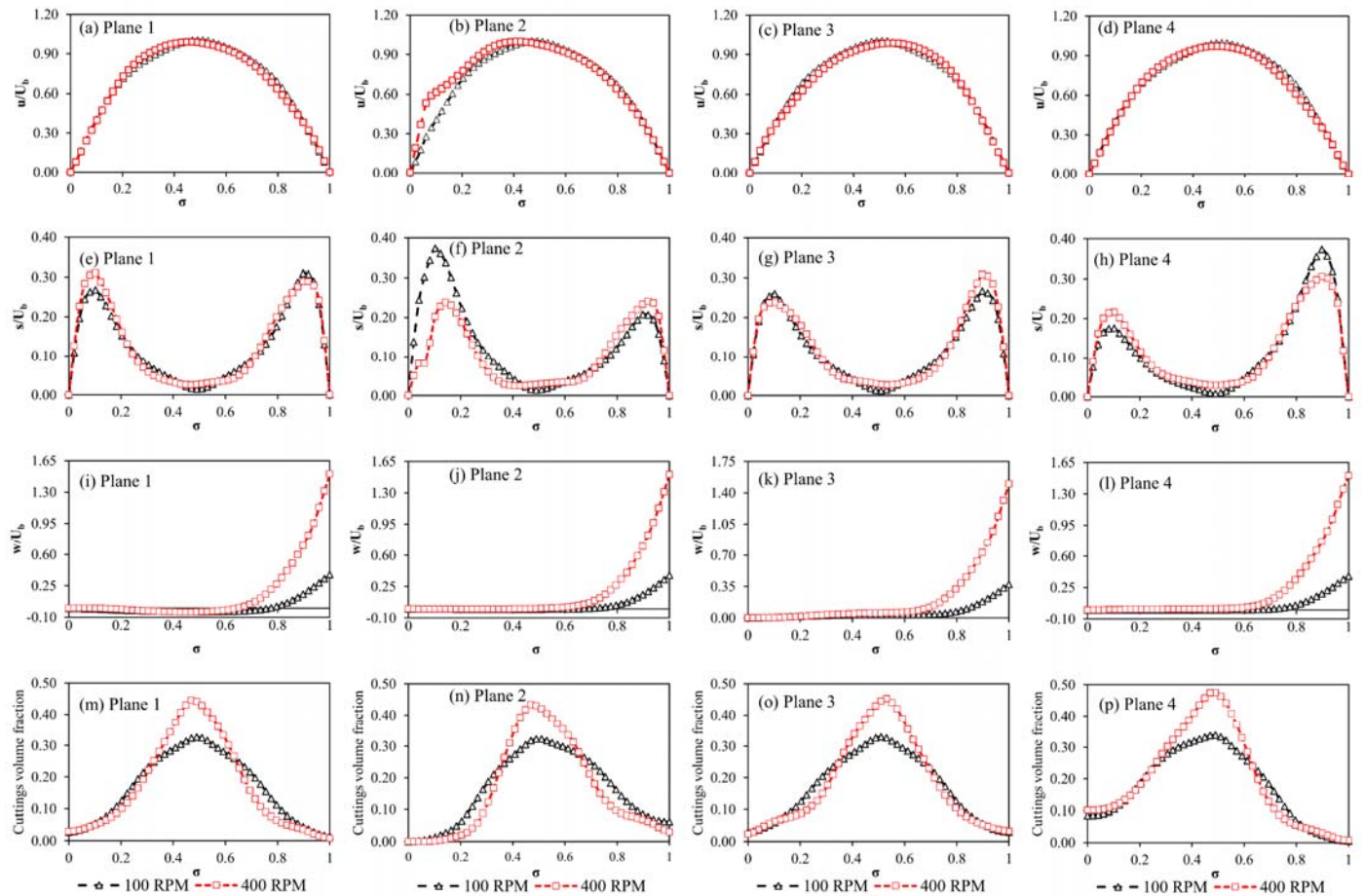

Fig. 7. Effect of drillpipe rotation on cuttings velocity profiles and volume fraction in a concentric annulus with the drilling mud as carrier fluid, wellbore inclination of 45°, ROP of 50 ft.hr^{-1} and 5 mm cuttings diameter.

3.1.2. Effect of wellbore inclination

Frictional resistance to flow or irreversible energy losses in the upward flow direction are much less in the liquid phase than in the solid phase; thus, the presence of slippage is unavoidable at any inclination for heterogeneous flows. Unlike the cuttings axial velocity profiles, slip velocities are more revealing with the change in hole inclination (Fig. 8e-h). It is observed that the horizontal configuration (90°), although with considerable portion of flow exposed to gravitational

13

resistance, shows the lowest slip in all planes. Conversely, the vertical flow configuration generally shows higher slip velocities. However, in planes 2 and 4 with strongest impact of pipe rotation as stated previously, we observe, the inclined configuration dominating in the magnitudes of slip velocities on different halves of the plane. Furthermore, tangential velocity profiles on these planes show very similar profiles; hence we resort to planes 1 and 3 for a better understanding of the impact of hole inclination on tangential velocity. Fig. 8i and 8k show that the resultant absolute tangential velocity of particles increases with the increase in inclination angle from the vertical. A plausible explanation for the negative tangential velocities observed could be that the effect of pipe rotation induces velocity fluctuations (but with a cuttings displacement pattern that keeps the streamline momentum).

Turbulent granular flows are characterised by incoherent and rapid shearing motions of the particles. Consequently, the boundaries of the flow domain generate energy at a rate equal to the product of the slip velocity and shear stress at the wall. Similarly, inter-particle interactions and particle interactions with the boundaries dissipate fluctuation energy via inelastic collisions. These energies can be transferred from one point to the other (granular conduction) in the annulus. The direction of granular conduction is determined by the wellbore inclination which in turn determines the solid fraction distribution in the flow (Ahn, 1985). The volume fraction profiles in Fig. 8m-p illustrate that fluctuation energy is being conducted from the base of the annulus (where energy is generated) to the bulk of the flow (where energy is mostly dissipated due to the high particle concentration and increased interactions). Hence, the solid fraction is low at the base, reaches a maximum towards the centre and then decreases near the drill pipe. Unless the energy generated supersedes the energy dissipated, there can be no sustained transport of the cuttings for a particular inclination, and cuttings build up becomes inevitable. The skewness in volume fraction as previously indicated in Fig. (7n and 7p) is seen to be replicated in Fig (8n and 8p).
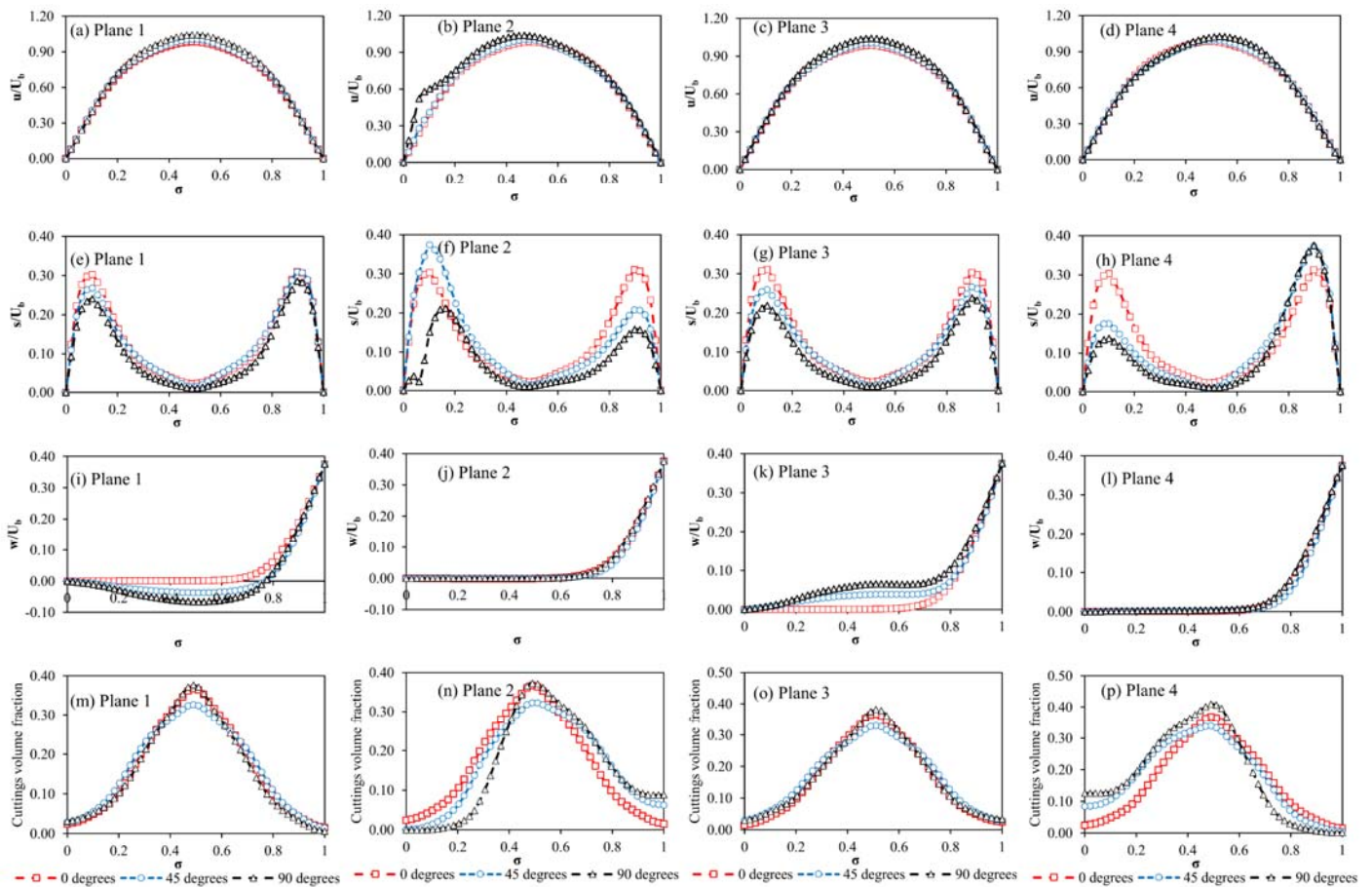

Fig. 8. Effect of wellbore inclination on cuttings velocity profiles and volume fraction in a concentric annulus with the drilling mud as carrier fluid, drill pipe rotation of 100 RPM, ROP of 50 ft.hr^{-1} and 5 mm cuttings diameter.

3.1.3. Effect of particle diameter

At this point, it is vital to consider the impact of the particles on the developed turbulent flow. When the response times of particles are short compared to typical times associated with the fluid motion, it is possible to have an

apparent alteration in the fluid's effective properties (effective density and viscosity). This is the case with the smallest (1mm) particles which tend to closely follow the fluid's turbulent motion. The results shown in Fig. 9a-d indicate that the cuttings axial velocity is to a large extent affected by the particle diameter. A greater dampening of the fluid's velocity is the case with very large particles (10 mm) as compared to smaller-sized particles (1 mm). A flatter velocity profile with high velocities, depicting the typical fluid turbulence is exhibited by smaller sized particles. This is further elucidated by the slip velocities in Fig. 9e-h, in which the slip velocities of the smallest particles are approximately two orders of magnitude lower than the slip velocities the 5 mm and 10 mm particles. The slip velocities observed with the 10 mm particles are evidently larger than the slip velocities experienced by the 5 mm particles. This could be explained by the mechanism of turbulence suppression which is as a result of the increase in velocity gradients in the flow (additional energy dissipation). However, a well-rounded indication of the particles' impact on flow turbulence should not only be thought of as a function of the velocity modulation they pose to the fluid; careful consideration of the disorderliness and chaotic structures they create in the flow as they interact with the continuous phase ought to be similarly made. The use of the Lagrange-Eulerian approach presented subsequently, pays more attention to the latter. The profiles of tangential velocities show that the larger particles possess higher tendencies to move along the rotating path of the drill pipe compared to the smaller particles (10 mm particles have the highest tangential velocities).

A complication present in annular flows as it relates to the conduction of fluctuation energy is that this energy (granular temperature) not only varies over the depth of flow but also with the radial and azimuthal positions along the annulus. The movement of particles to regions originally devoid of particles (spreading) is observed with the 1mm diameter particles thus further demonstrating its tendency to behave in a continuous manner as the carrier fluid. The profiles of the 1mm particle volume fraction show two mild off-centre peaks at regions close to the walls which possibly signify the even spreading limit of the small cuttings in the annulus.
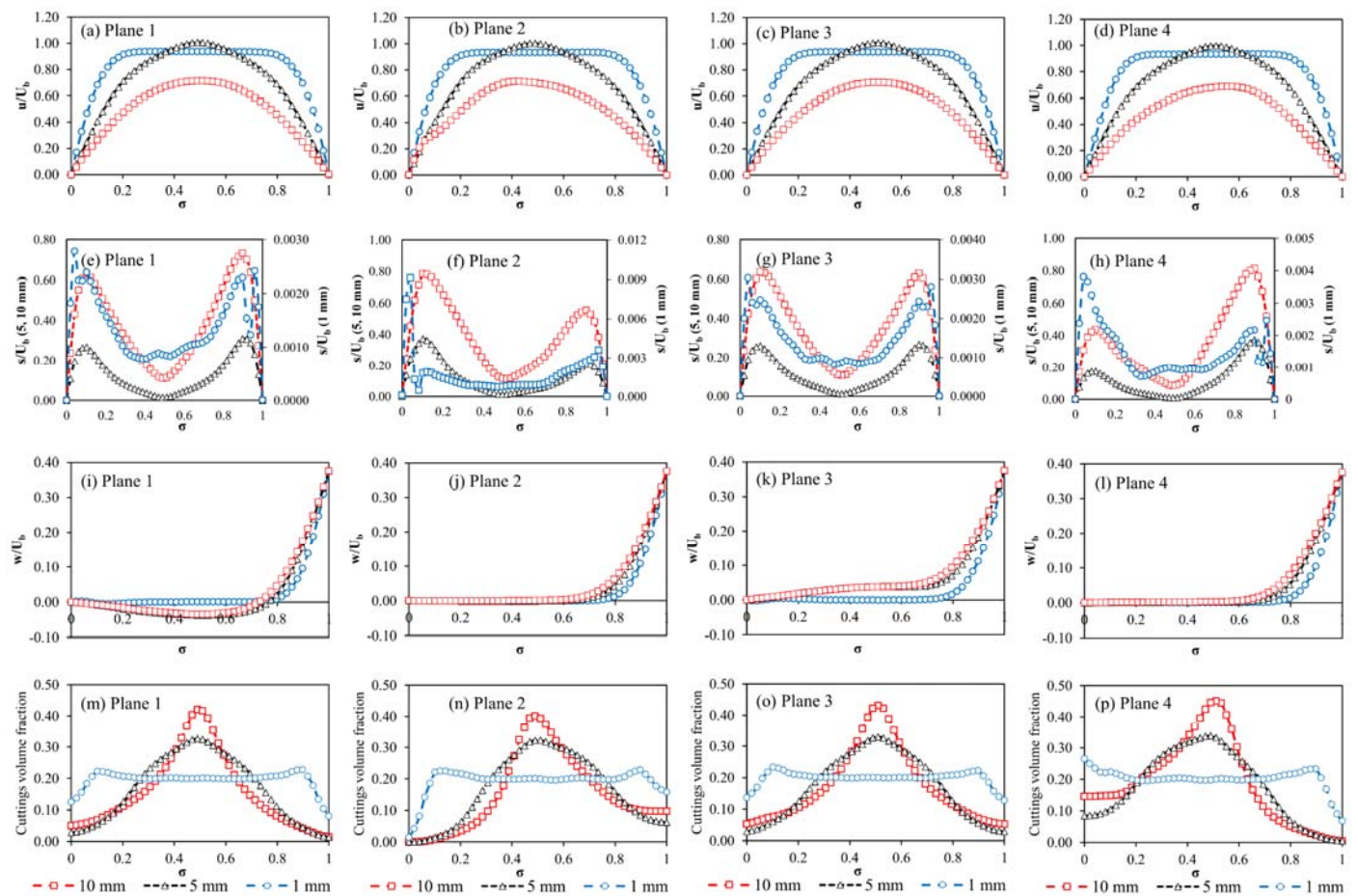

Fig. 9. Effect of particle diameter on cuttings velocity profiles and volume fraction in a concentric annulus with the drilling mud as carrier fluid, wellbore inclination of 45°, ROP of 50 ft.hr^{-1} and drill pipe rotation of 100 RPM.

3.1.4. Effect of fluid rheology

Water, a less viscous fluid compared to the drilling mud lacks the viscosity/suspension ability to sustain the continuous transport of cuttings in the annulus. Hence, the cuttings move at a lower velocity compared to the drilling mud along the main flow axis Fig. 10a-d. The slip velocities noticed with water also indicate that water hardly overcomes the large cuttings density during transport thus causing an increased drag on the solids phase against the direction of flow. This is further reflected in the high volume fractions exhibited by the cuttings Fig. 10m-p. This is more evident in plane 4 (the bottom section of the 45° inclined annulus) which is more susceptible to the impact of gravitational resistance. On the other hand, the tangential velocity profiles of the cuttings with water are generally higher than that of the mud. This is also illustrated in the fluid velocity streamlines shown later on with the DPM/DEM model (Fig, 14f). While the use of water induces an increased circular motion in the annulus due to its relatively lower viscosity, the drilling mud has the bulk of its velocity magnitude channelled towards the axial direction. There is thus a clear outperformance of water by the drilling mud.

3.2. Analysis of velocity profiles in an eccentric annulus using the Eulerian-Eulerian Model

As in the concentric case, same parametric variation is carried out in the eccentric annulus. Although most of the already observed and discussed phenomena are replicated here, there are subtle differences in the velocity and volume fraction profiles and they carefully examined next.

3.2.1. Effect of drill pipe rotation

As expected, increased frictional resistance is responsible for the lower velocities experienced by cuttings in the lower part of the annulus (Fig. 11d). Also shown in Fig 11d is the stronger impact of drillpipe rotation in the lower part of
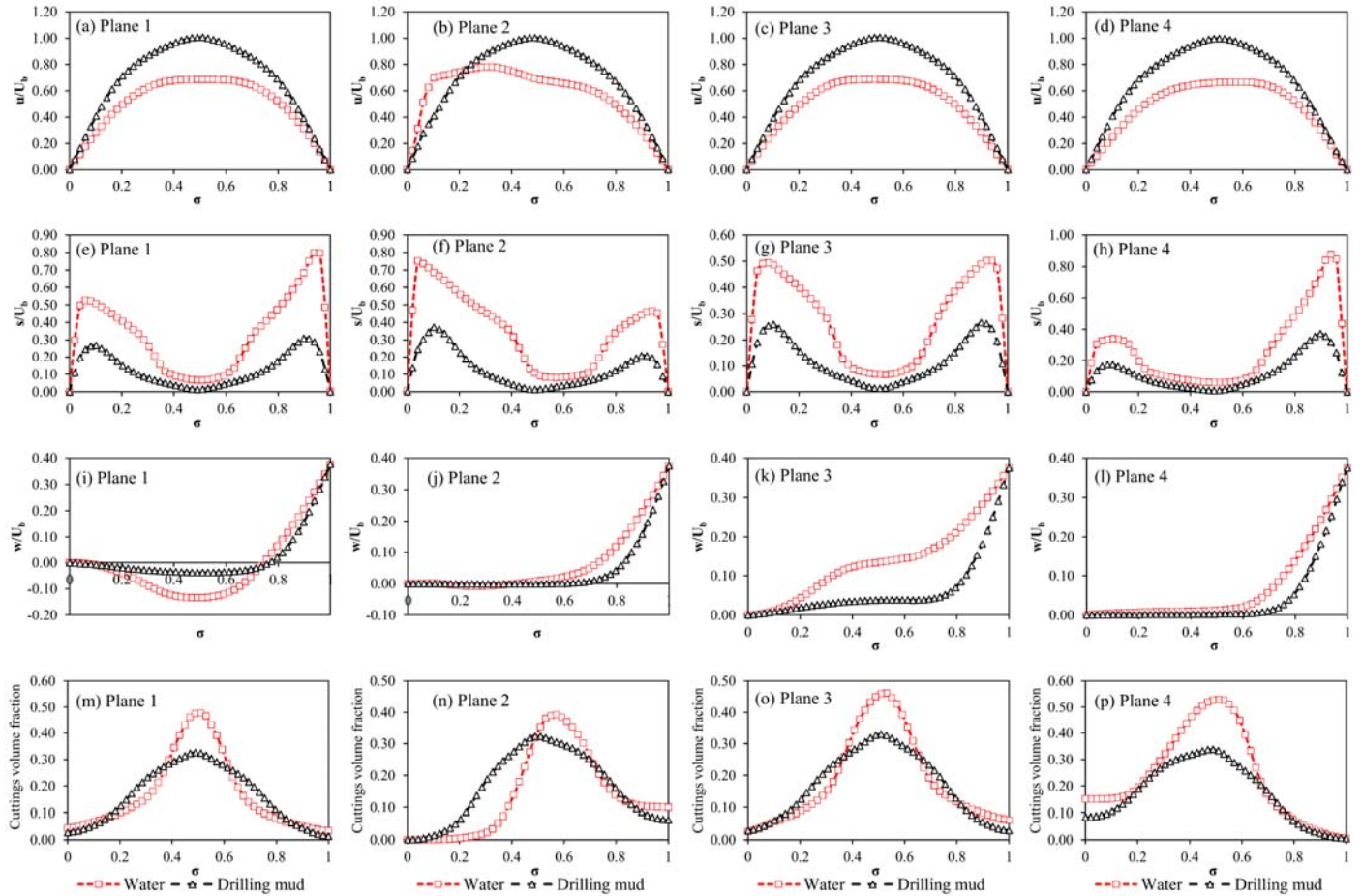
the eccentric annulus (Plane 4) compared to other regions. Tangential velocity is seen to increase with inner pipe rotation; thus low velocity cuttings close to the inner pipe and at the base of the annulus are swung into the bulk flow region. Asides the clearly illustrated trend that explains that increased rotation causes a reduction in slip velocity, it can also be observed that the slip velocity profiles of the eccentric annulus display a more sustained central flattened region compared to the concentric annulus (except in plane 4). It could therefore be argued that the effect of drill pipe rotation is stronger in the eccentric annulus than the concentric annulus. This is because the shear thinning behaviour of the non-Newtonian fluid makes it experience viscosity variations around the eccentric annulus with varying shear rates.

Fig. 10. Effect of fluid rheology on cuttings velocity profiles and volume fraction in a concentric annulus at a wellbore inclination of 45°, ROP of 50 ft.hr^{-1}, drill pipe rotation of 100 RPM and 5 mm cuttings.

In the wider part of the annulus (low-shear region), the viscosity of the fluid is relatively higher, thus leading to an increase in its carrying capacity. Conversely, at the narrow annular section (high-shear region), the viscosity is lower and a reduction in the fluid carrying capacity ensues. The concentric annulus however, experiences a pseudo-uniform shear rate with similar fluid performance irrespective of cuttings location. This increased shear thinning effect with increased pipe rotation is also the most probable reason for the slightly reduced cuttings velocity (at 400 RPM – Fig. 11d). Furthermore, while the extended flattened central regions are relatively similar for both rotations in the eccentric annulus; this is not the case in the concentric annulus slip velocity profiles (Fig 7e-h). At 400 RPM, the central part is more flattened compared to the slip velocities at 100 RPM (Fig 7e-h). Thus the impact of drill pipe rotation could be advantageous in that slip velocities are reduced, but can be unfavourable (specifically at the lower parts of the annulus) due to increased shear thinning in eccentric configurations. The coupled manifestation of both phenomena could be the reason why various researchers (Ofei et al. 2014; Han et al. 2010; Duan et al. 2008) have discovered only slight improvements in cuttings transport efficiency when drill pipe rotation is increased. The volume fraction/distribution of solids are distinct in each plane with off-centre peaks appearing in both drill pipe rotations. Furthermore, solid phase volume fractions close to the drill pipe and wellbore are less than other regions; this allows faster fluid movements relative to the solid, hence the two peaks experienced in the slip velocity profiles. It is however noticed that the dual peaks in volume fraction profiles (Fig. 11m-o) which are most likely attributable to the eccentric flow configuration are absent in Plane 4 – the bottom of the annulus. Inevitably, this occurs due to the build of cuttings (reflected in the higher volume fractions – Fig. 11p).

3.2.2. Effect of wellbore inclination

The cuttings axial velocity profiles illustrate that the horizontal flow configuration slightly favours the transport of cuttings (Fig. 12a-c); however, slip velocities show more pronounced effects with changes in the hole inclination. As observed, the slip velocities are lowest in the horizontal annulus.
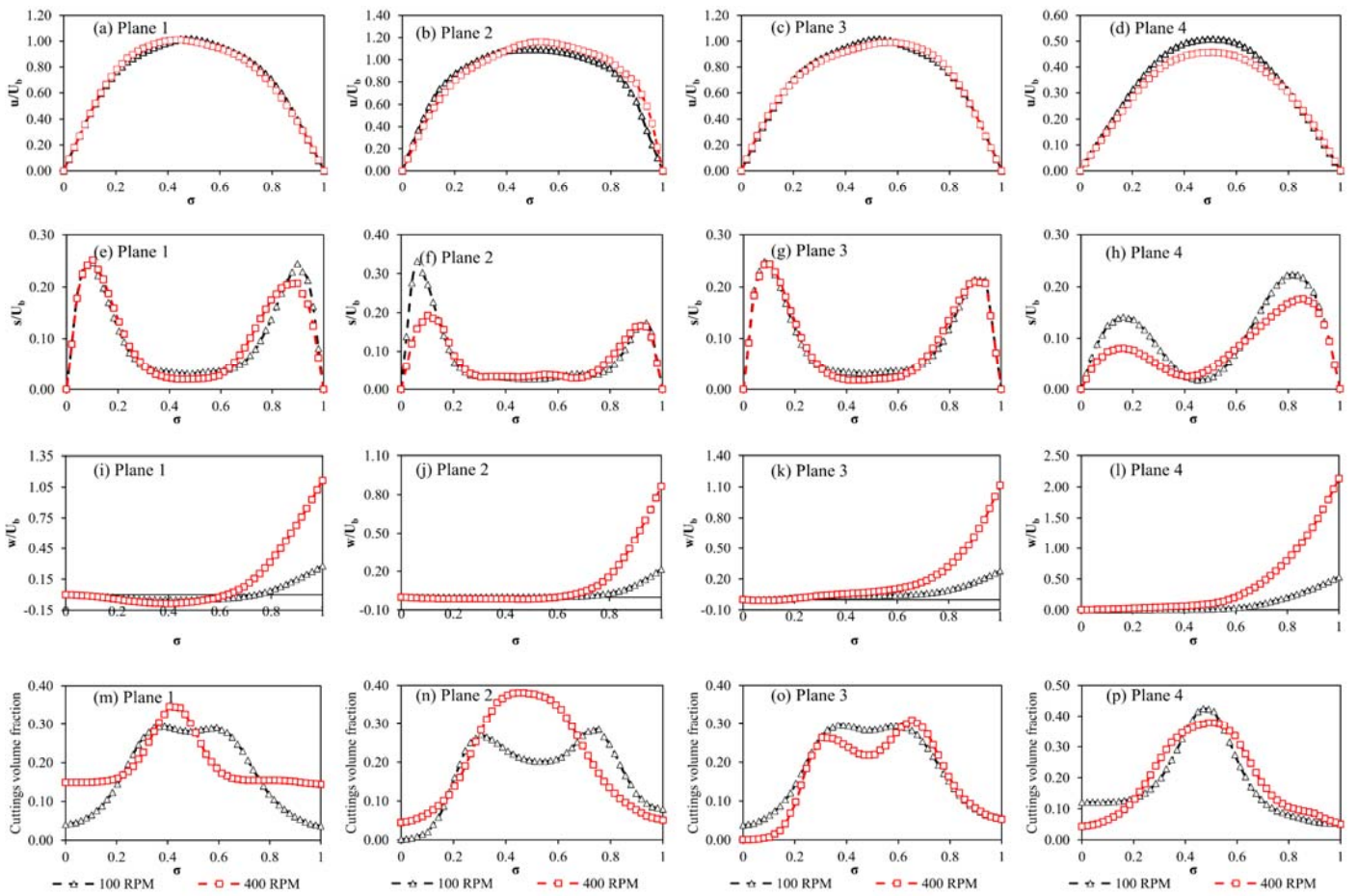
Fig. 11. Effect of drillpipe rotation on cuttings velocity profiles and volume fraction in an eccentric annulus with the drilling mud as carrier fluid, wellbore inclination of 45°, ROP of 50 ft.hr^{-1} and 5 mm cuttings diameter.
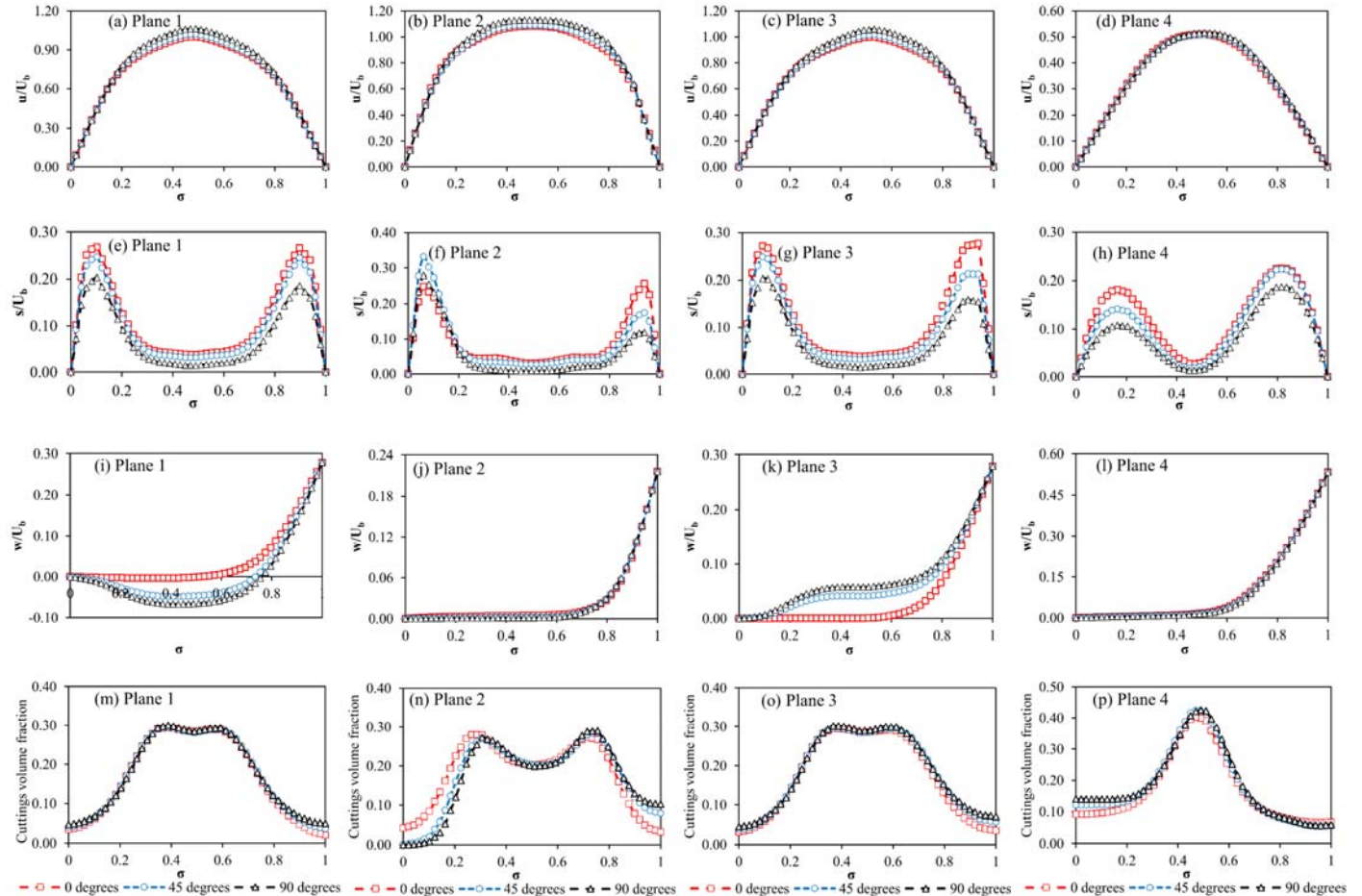

Fig. 12. Effect of wellbore inclination on cuttings velocity profiles and volume fraction in an eccentric annulus with the drilling mud as carrier fluid, drill pipe rotation of 100 RPM, ROP of 50 ft.hr^{-1} and 5 mm cuttings diameter.

This is because the impact of gravitational flow resistance on the density difference between both phases is not as high as when the wellbore is inclined or vertical. Additionally, the impact of pipe rotation reflected in the tangential velocities (Fig. 12i-l) is higher in the horizontal and inclined annulus compared to the vertical configuration. A possible reason for this, is that the improvement in cuttings transport phenomena is very noticeable for a system characterised by relatively large velocity gradients (some particles moving with bulk fluid and others gliding over a bed or stationary, such as the case in horizontal or inclined annuli). On the other hand, a flow system in which these gradients are relatively lower, does not seem to experience to the same degree, the impact of drill pipe rotation (which is to sweep cuttings from the narrower region to the wider region in the annulus). For the same previously explained reasons, the narrower section shows higher tangential velocities. Except for plane 4 with the highest volume fraction, the dual off-centre peaks in volume fraction are exhibited by all inclination angles in planes 1, 2 and 3 (Fig. 12m-p).
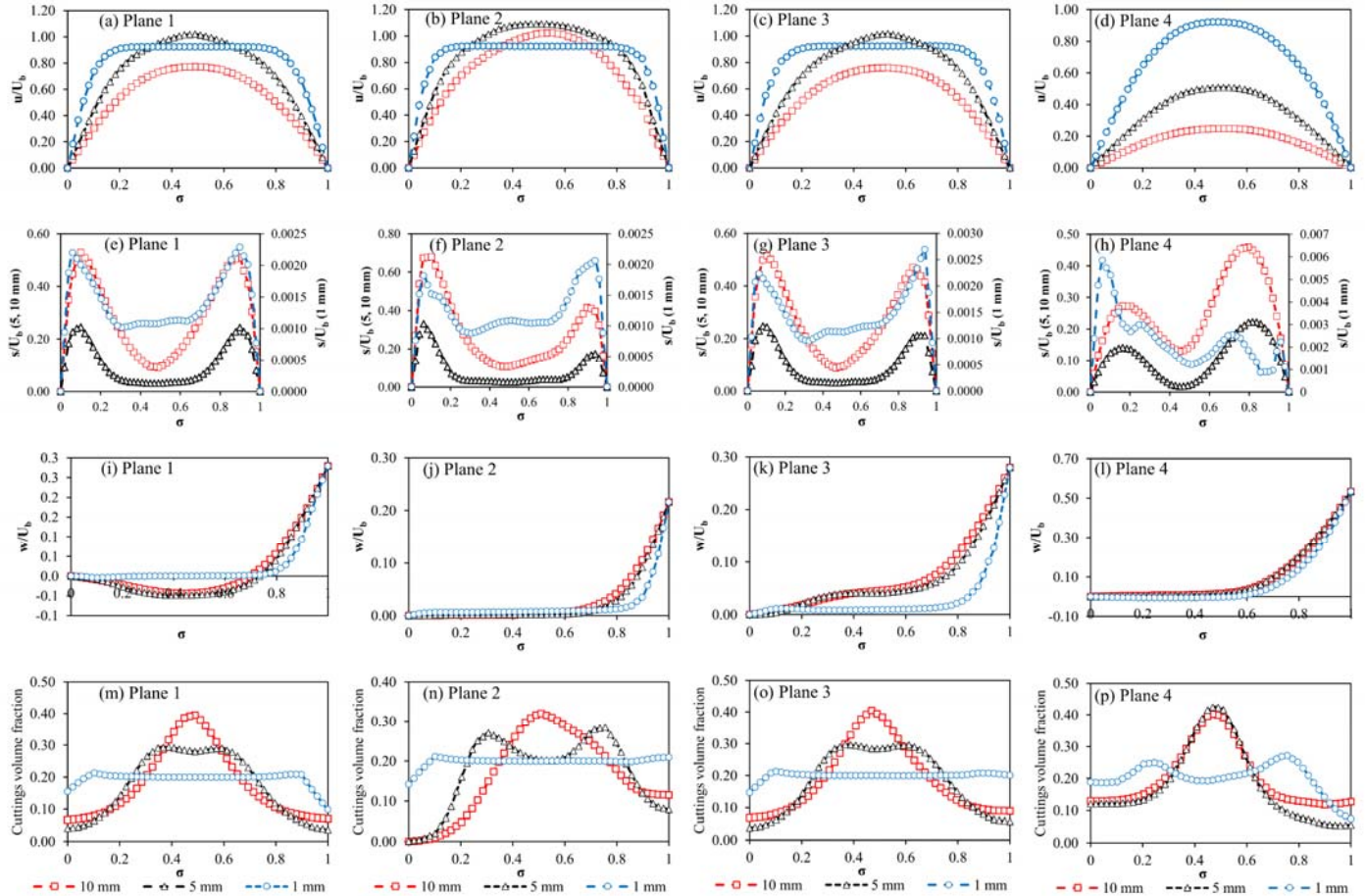

Fig. 13. Effect of particle diameter on cuttings velocity profiles and volume fraction in an eccentric annulus with the drilling mud as carrier fluid, wellbore inclination of 45°, ROP of 50 ft.hr^{-1} and drill pipe rotation of 100 RPM.

3.2.3. Effect of particle diameter

Particle spread around the annulus is higher with the 1mm particles than other particle sizes. Consequently, at the bottom of the annulus, smaller particles travel fastest (Fig. 13d). Not only do the 5mm particles exhibit lower slip velocities, they also have a more flattened profile at the central part of the annulus compared to the 10mm particles; hence demonstrating their relative ease of transport. The 1mm particles on the other hand, have very low slip velocities (about 2 orders of magnitude less than the other particles). Similar to the concentric case, larger particles show greater tendency to rotate along the circular path of the drill pipe compared to the 5mm and 1mm particles. Also, the cuttings distribution along all planes illustrate the spreading tendencies of the individual particle sizes. 10 mm particles have their peak concentrations in the middle of the annulus with a steep-sided drop until the boundaries are reached; whereas, 1mm particles show a fairly constant concentration throughout, but drop abruptly close to the walls. Smaller particles will tend to respond faster to the fluid flow and would faithfully follow the fluid path lines compared to larger particles. Larger particles, due to increased inertia effects will take a relatively longer time to respond to the fluid flow and hence would most likely continue in near rectilinear trajectories or independent random trajectories that impose more turbulence to the flow. The explained phenomena is observed in the trajectories of particles shown in Figure (17b) which further explains the spreading phenomena.

3.2.4. Effect of fluid rheology

Asides the occurrence of dual off-centred peaks in the volume fraction profiles of the eccentric annulus (Fig. 14m-p), all other profiles and explanations are similar to the concentric annulus. For the range of varied parameters, no volume fraction profile in the concentric annulus portrayed the dual-peak phenomenon; hence, its occurrence is most likely due to the peculiarities of the shearing mechanism and granular conduction in the eccentric configuration.
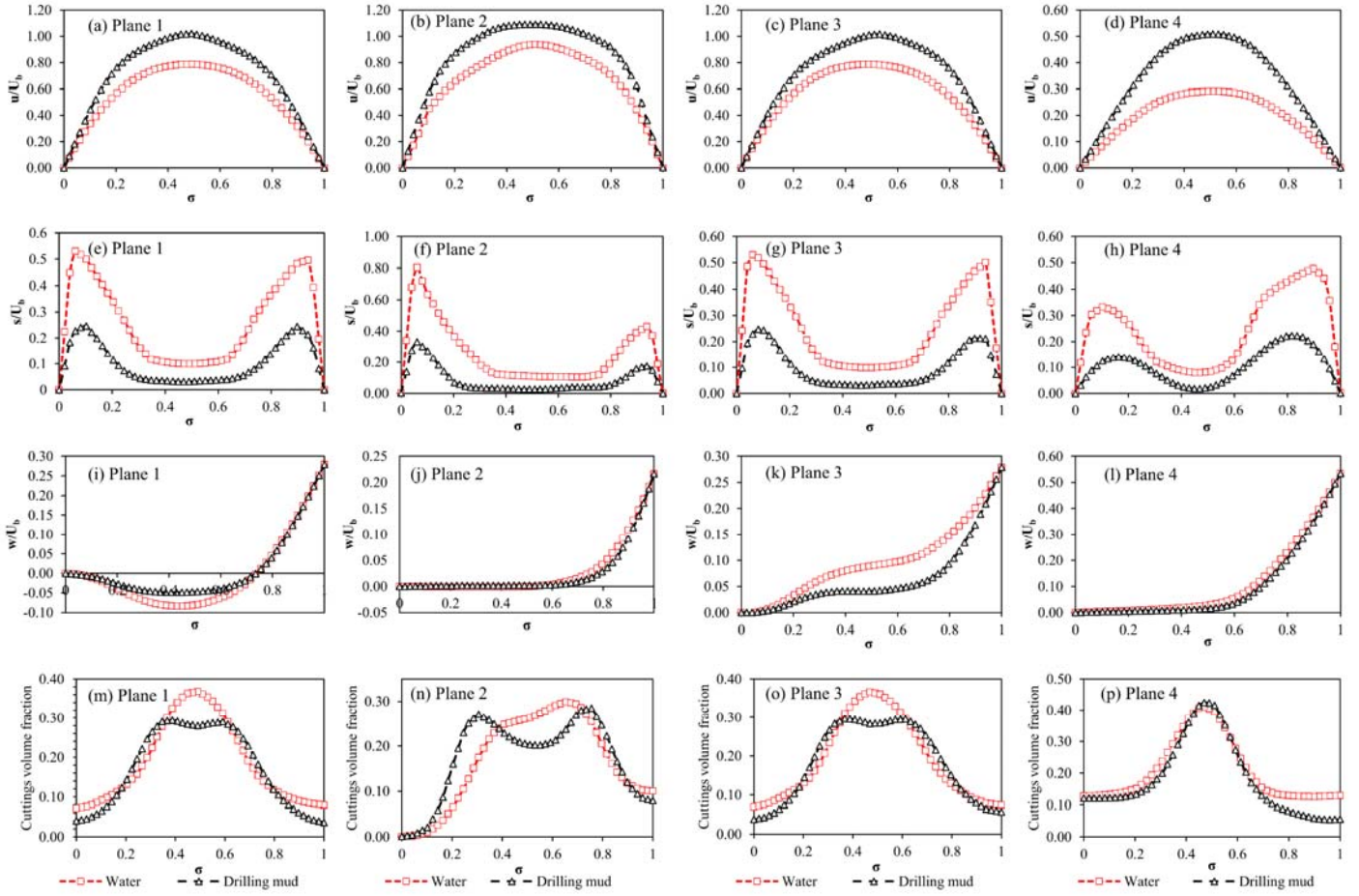

Fig. 14. Effect of fluid rheology on cuttings velocity profiles and volume fraction in an eccentric annulus at a wellbore inclination of 45°, ROP of 50 ft.hr^{-1}, drill pipe rotation of 100 RPM and 5 mm cuttings.

3.3 Analysis of pressure drop profiles for the concentric and eccentric annulus

Fig. 15 shows the pressure drop profiles for the different flow configurations. With increase in pipe rotation, only a slight increase in pressure drop is observed in the concentric annulus. The eccentric annulus however, shows no difference. The slight increase is attributable to the shear instabilities that ensue as a result of the rotary motion of the drill pipe. The impact of gravity in both annuli is the inevitable reason for the higher pressure drop values noticed with the vertical configuration. Pressure drop is seen to reduce as the annulus becomes horizontal. Furthermore, increased particle inertia with increased particle size and collision frequency indicate a higher pressure drop is necessary for their transport. Thus, 10mm particles have the highest pressure drop in both concentric and eccentric annuli; compared to the eccentric wellbore, the 10mm particles in the concentric configuration induce a pressure drop which is considerably higher than those observed with the smaller sized particles - 1mm and 5mm (Fig. 15c and 15g). Viscosity differences between the drilling mud and water and thus the shear forces majorly constitutes the reason for the increased pressure drop associated with the mud. Better hole cleaning is achievable with the use of the mud compared to water as the carrier fluid.

3.4 Analysis of particle trajectory using the Lagrangian-Eulerian model

Although, the Eulerian-Eulerian approach earlier seen requires transport quantities of all phases to be continuous throughout the computational domain, in reality, these phases could be time dependent and as well, be discretely distributed. In this section, we address flow conditions in which the direct inter-particle and particle-wall interactions play the most important role in determining the flow mechanics. Through the consideration of time dependency and the use of appropriate boundary conditions, it is possible to gain better insight into the transport phenomena; one of which is the combined effects of turbulence and gravity on particle settling. Only the eccentric configuration is considered in this case due to its greater prevalence in drilling operations and the computational expense involved.

Except where specified, particle diameter = 5mm; drill pipe rotation = 100 RPM, ROP = 100 ft.hr^{-1}; wellbore inclination = 90° (horizontal wellbore); and the carrier fluid is drilling mud.

3.4.1. Analysis of fluid streamlines

Fig. 16 shows the streamlines of the fluid velocities at different flow conditions after a simulation time of 3.5 seconds (sufficient for the attainment of SSS). The wider annular sections generally display high fluid velocities due to the
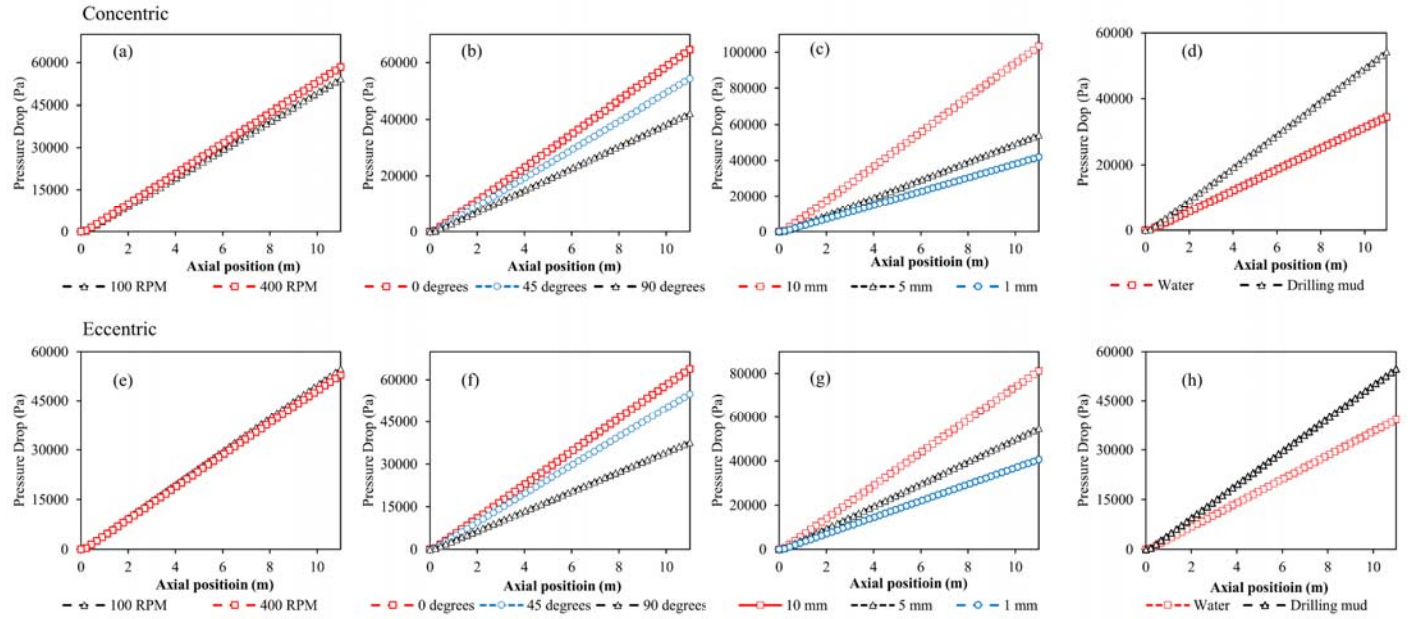
lower.

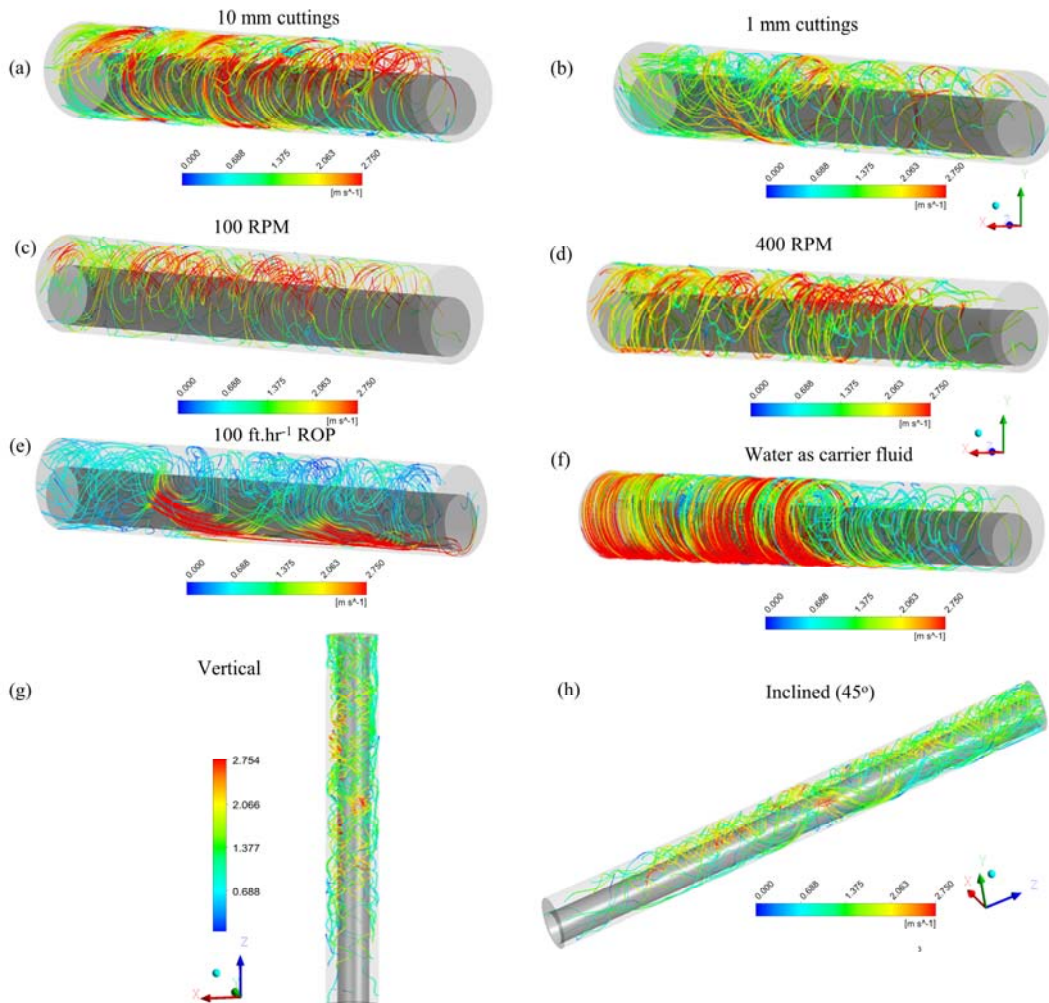F**ig. 15.** Pressure drop profiles

Fig. 16. Fluid streamlines at different flow conditions

flow resistance encountered. In the case where 1mm particles are used, a relatively large region of lower fluid velocities is noticed. This is because the particles assume a more continuous flow mechanism thus, altering the effective fluid viscosity. With wellbore inclination (0° and 45° from the vertical), the fluid velocity is hindered by gravitational resistance. At a drill pipe rotation of 400 RPM, the swirling frequency of the fluid increases as shown in the slightly more concentrated streamlines of (Fig 16d). Furthermore, when water is used as the carrier fluid, a highly circumferential transport mechanism is noticed comparted to other flow conditions (Fig. 16f). This further substantiates the observations of tangential velocity profiles seen in Fig. 10i-l and 14i-l. A higher Rate of Penetration (ROP) implies more cuttings ingress which causes an increase in the shear rate particularly at the bottom of the annulus where the particles tend to settle; this is depicted as the high velocity region at the bottom of the annulus (Fig. 16e) compared to other regions.

3.4.2. Analysis of particle streamlines

Compared to the rather continuous fluid streamlines, those of the particles are highly discontinuous (Fig. 18a-h), thus explaining the haphazard motion of the particles associated with the turbulent motion of the fluid. Particles generally displayed oscillatory movements due to pipe rotation from the animations of particle tracks developed. The inclined, vertical and 100 ft.hr^{-1} (ROP) flow conditions revealed pronounced reverse flows in particle motion. The reasons are of course related to the impact of gravity and increased particle ingress into the annulus. The impact of rotation on the 10mm particles appears to be the strongest (Fig. 18a). The streamlines (Fig. 18a) show that the particles traverse the circular path to a greater extent compared to the 1mm and 5 mm particles. Again this was demonstrated in the tangential velocity profiles using the Eulerian-Eulerian model (Fig. 9i-l and 13i-l). A high interpenetration of particle lines at the sides of annulus is observed with the 1mm particles (Fig. 18b); the degree of this particle dispersion can be scaled with the Stokes number (Roco, 1993). Figure 16 shows the calculated Stokes numbers and turbulent eddy frequencies for the different particle diameters. Chien and Chun, (1987) observed that a Stokes number close to unity indicates the tendency of particles to attain maximum spread in the flow domain; which corresponds with results obtained so far with the EE model. However, Tang et al. (1992) discovered a rather dramatic phenomenon in which large scale turbulent structures could lead to an organised concentration pattern of small sized particles in localised regions of the flow; thus demonstrating that the existence of turbulence does not always guarantee the production of homogeneous mixture. This is a reasonable explanation for the observed structures along the sides of the annulus for the 1mm cuttings Fig (17b). The turbulent eddy frequency was used as an index of the particles' impact on fluid turbulence. As clearly illustrated in Fig. 17, larger particles exhibit the highest frequency thus, implying a greater tendency to induce turbulence. The 5mm particles follow next in magnitude, while the smallest particles exhibit the lowest frequencies. With the results obtained from the Eulerian-Eulerian model and the Lagrangian-Eulerian model, we infer that modulation/dissipation of fluid turbulence and the generation of additional turbulence to the flow are intricately dependent on the particle size.
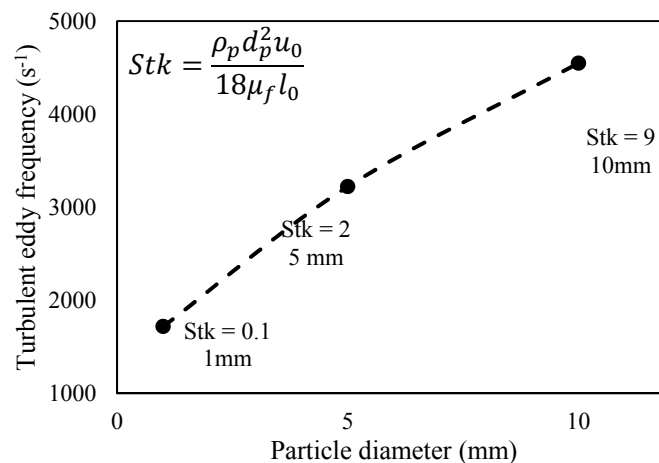

$$Stk = \frac{\rho_p d_p^2 u_0}{18 \mu_f l_0}$$

Fig. 17. Contribution of particles to the turbulence of flow

Although the impact of hole eccentricity in the vertical flow configuration is relatively less significant, Fig.17g shows that particles tend to travel along the sides of the annulus. The wider region of the annular space leaves a large section of the flow open to gravitational resistance compared to sides, thus explaining the most likely reason for the observed transport mechanism. Observed velocities in the vertical and inclined annulus are generally lower than those observed in the horizontal flow conditions.

3.4.3. Analysis of fluid velocity vectors along the longitudinal plane (YZ)

Asides affecting the unsteady nature of the shear layer, the occurrence of particles can also affect the growth and vorticity profiles in the developing layer thus giving rise to some organised structures in the fluid. Analysing the velocity vectors of the fluid in both normal and tangential directions along the longitudinal YZ Plane (Fig. 19) could provide deeper insight into the underlying phenomena. Kline et al. (1967), Hetsroni, (1989) and Roco (1993) pointed out the formation of coherent structures at the wall (organised streak-like fluid structures moving at different velocities due to shearing forces) visually observed in two phase solid-liquid flows; it was also discovered that turbulence energy production is a consequence of this phenomena. These streak-like strictures observed in Fig. 19, originate from the wall and generally lift particles into the bulk flow region. After these ejected particles move a certain distance from the wall, they experience a loss in their upward momentum and return towards the wall. This occurs continuously throughout the flow and is termed 'particle recycling' (Iyoho et al. 1986; Crowe et al. 1985). The frequency of these ejections from the boundaries significantly depends on the particle properties. As flow progresses, eddies developed by the particle-fluid interaction in the bulk flow are transformed into higher frequencies turbulent motion depending on the magnitude of the slip velocity; thus larger particles may cause increased formation of these coherent structures.
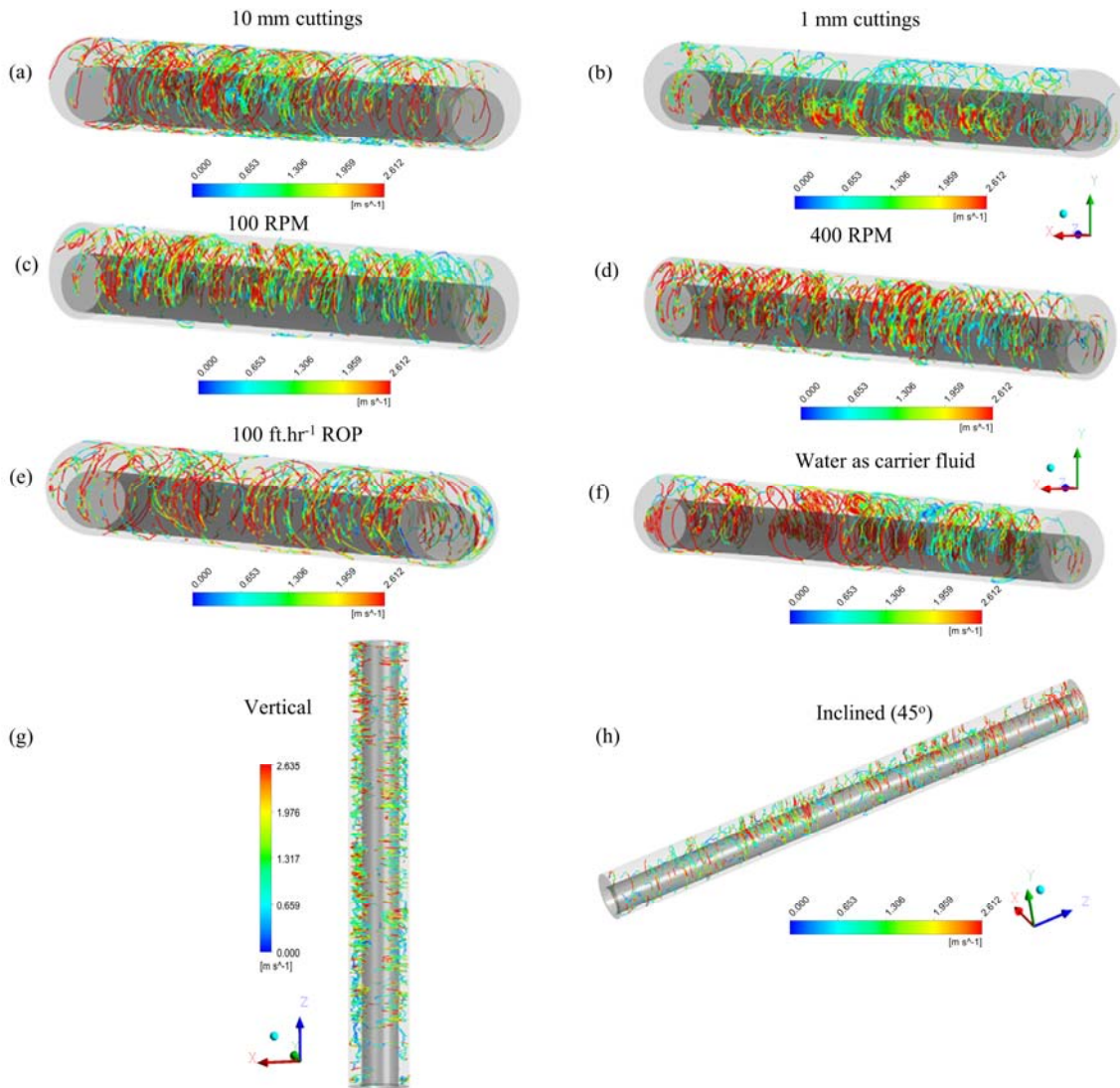

Fig. 18. Cuttings streamlines at different flow conditions

3.4.4. Analysis of cuttings volume fraction

Time averaged volume fractions over a simulation time of 3.5 seconds are displayed in Fig. 20. Particle volume fraction is seen to increase at the narrower annular section in virtually all flow configurations asides the vertical (in which particles concentrate around the sides). The use of water as the carrier fluid results in higher particle deposits; this deposition increases further when a drilling mud is used but at a higher penetration rate of 100ft.hr^{-1}. High rates of penetration induce increased fluctuations in particle velocity which prevent free particle movements from one annular

location to another, thus increasing the velocity gradients and eventual deposition tendencies. Animations produced from the simulation of the cuttings transport phenomena at high ROP reveal considerable reverse flow in particle motion which is pronounced at the entry up until mid-way the annulus. A further explanation to the impact of high ROPs is that the friction at particle-particle and particle wall contacts becomes higher; hence slip occurs and relatively higher tangential velocity is imparted to the particles which causes an increase in the granular temperature. As previously explained, a local concentration of the 1mm particles occurs along the lateral annular section. The impact of pipe rotation is seen to affect the particle distribution particularly at regions close to the entrance of the annulus.
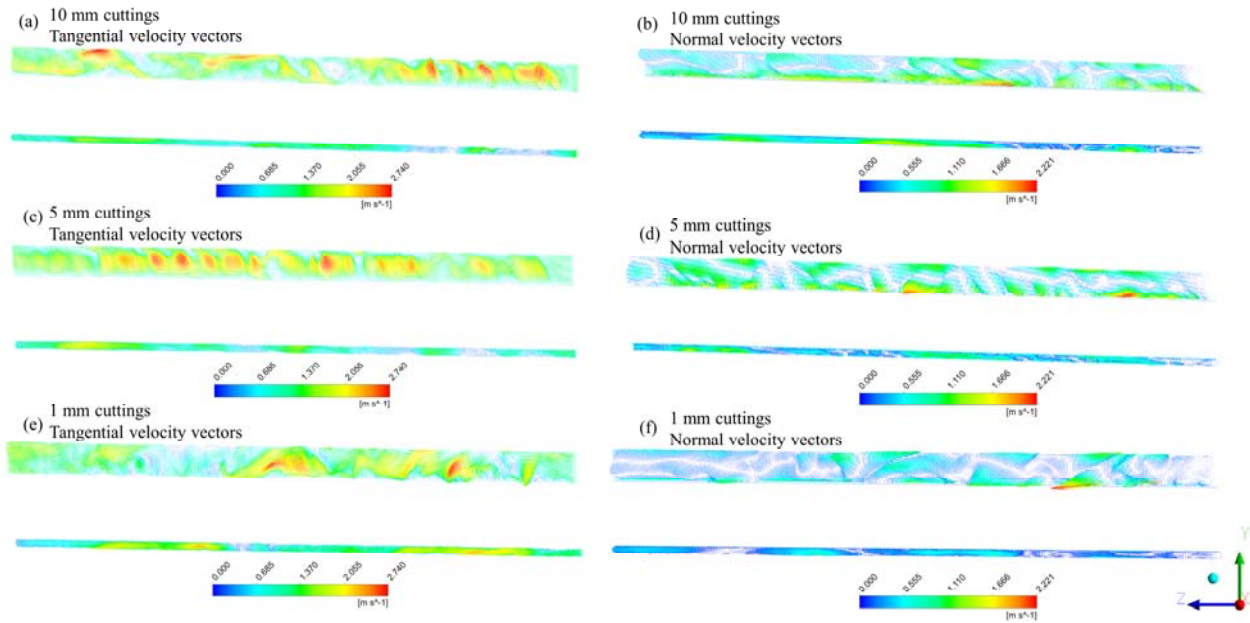
Accurate determination of hole cleaning performance significantly depends on the predictability of cuttings annular distribution under different drilling conditions and this has so far been demonstrated.

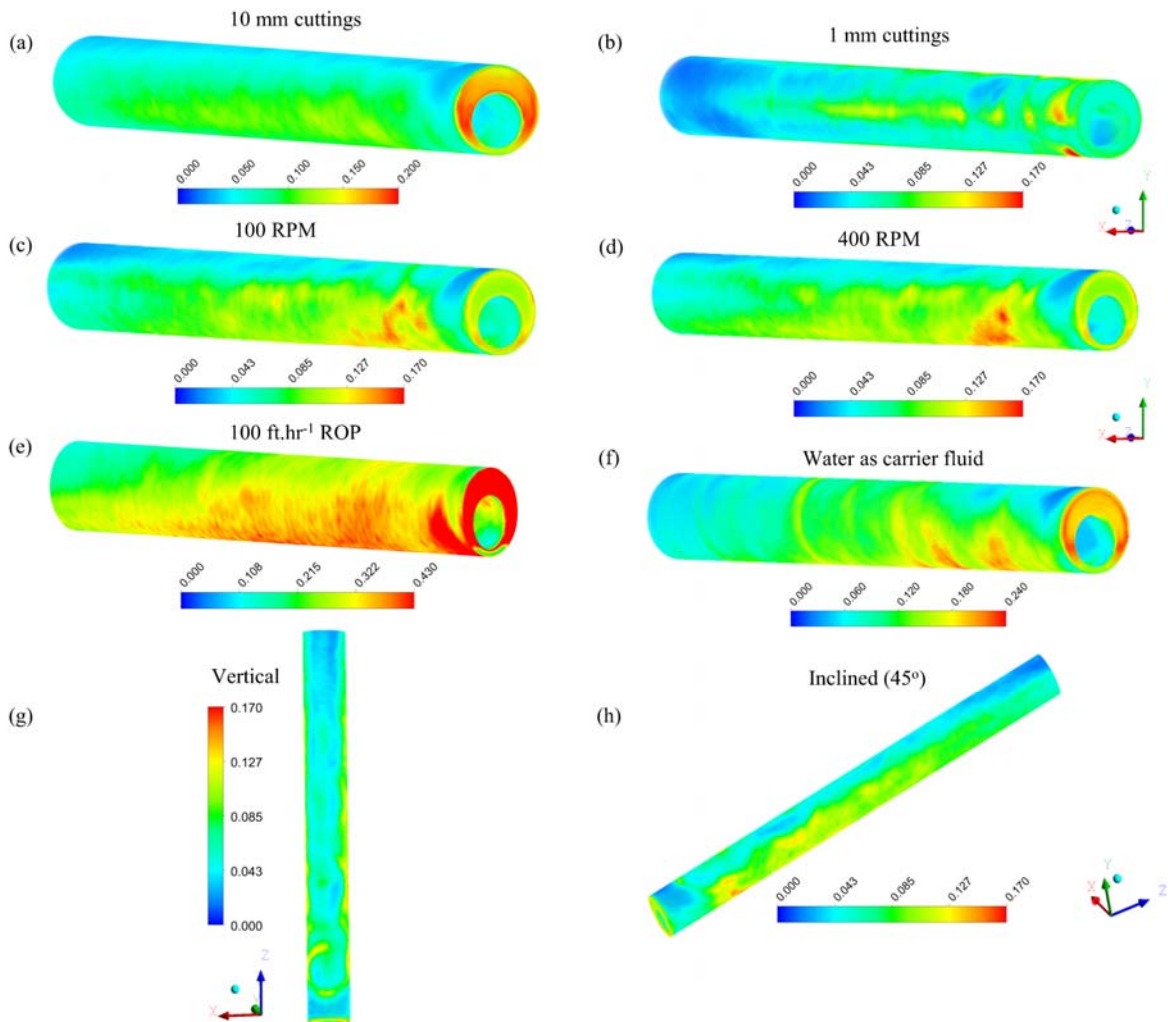**Fig. 19.** Fluid velocity vector plots showing ejections from the walls

Fig. 20. Cuttings volume fraction at different flow conditions.

4. Conclusions

This paper presents the steady and unsteady state analysis of drill cuttings transport phenomena under turbulent conditions using the Eulerian-Eulerian and Lagrangian-Eulerian multiphase modelling methods. It was discovered that the complex boundary phenomena that evolve in multiphase flows containing solid particles cannot be understood independently of the flow field and thus an evaluation of the velocity and volume fraction profiles at different flow conditions was carried out. Further observations made during this study lead to the following conclusions.

- Slip velocity profiles generally displayed a convex signature in the central regions of all annular planes considered. Increased pipe rotation (400 RPM) in the concentric annulus is seen to yield more flattened central profiles compared to lower rotation velocities of 100 RPM. Drill pipe rotation thus aids homogeneity in cuttings removal.
- The tangential velocity experienced by particles is higher when the flow configuration is horizontal. Also, large (10 mm) particles tend to closely follow the rotational motion of the drill pipe compared to cuttings of smaller sizes (1mm and 5mm).
- We infer that there is some slight modification of the effective fluid properties (increased viscosity and density) by the cuttings of 1mm diameter (very low Stokes number). Hence the lower fluid velocities observed compared to other particle diameters.
- The profiles of volume fraction using the Eulerian-Eulerian model show that 1mm particles are more readily dispersed around the annulus compared to larger particles. While the 10mm particles tend to dampen the flow turbulence as demonstrated in the cuttings axial velocity profiles, they may also enhance turbulence by increasing occurrence of large and small scale eddies. Turbulent eddy frequencies were observed to be larger with particles of 10mm diameter compared to when the (1mm and 5mm particles are used).
- The occurrence of coherent structures (streak-like fluid ejections emanating from the wall) is observed using the Lagrangian-Eulerian model. These structures are mainly responsible for the lifting of particles into the bulk flow region. It is also possible that these structures are enhanced by the effect of drill pipe rotation.
- Particle streamlines, and 3D volume fraction profiles in the vertical flow configuration reveal that particles tend to travel along the sides of the annulus compared to other annular regions.

While experimental measurements of cuttings velocity during high speed turbulent flows with high Stokes numbers could be difficult to obtain because of the increasing gravitational effects for large particles, CFD methods demonstrated in this work shows remarkable potential for predicting and understanding such flow conditions in a more cost-effective way. Although major progress has been made, a lot still remains to be done; particularly investigating new phenomena surrounding flows with non-uniform particle size distribution and the occurrence 3 phases (solid, liquid and gas) during underbalanced drilling operations. Consequently, more experimental data on cuttings velocity profiles would be necessary for further validation of CFD models.

5. Nomenclature

Latin letters

$A_{annulus}$	Drill pipe cross sectional area (m^2)	$\vec{g}$	Gravitational acceleration (m.s^{-2})
AR	Aspect Ratio (-)	$g_{0,ss}$	Compressibility transition function (-)
C_l	Lift coefficient (-)	I_{2D}	Second variant of the deviatoric stress (-)
C_D	Drag coefficient (-)	$\vec{K}_{pf}$	Interphase momentum exchange coefficient (-)
c_p	Cuttings concentration (%)	K	Consistency index (Pa.s^n)
CMC	Carboxymethyl cellulose solution	$\dot{m}$	Mass flow rate (kg.s^{-1})
D_{pipe}	Drill pipe diameter (m)	n	Flow behaviour index (-)
D_{wb}	Wellbore/Hole diameter (m)	p_p	Solids pressure (Pa)
d_p	Diameter of solids (m)	r	Annular distance
e	Eccentricity (-)	R_{in}	Drill pipe radius (m)
e_{ss}	Coefficient of restitution (-)	R_o	Wellbore radius (m)
$\vec{F}$	Additional force term (N)	ROP	Rate of Penetration (ft.hr^{-1})
F_D	Drag force (N)	Re_p	Solid particles Reynolds number (-)

Re_{ω}	Vorticity Reynolds number (-)	$\vec{v}_f$	Fluid phase velocity (m.s^{-1})
Re_s	Relative Reynolds number (-)	$\vec{v}_{f,x}$	Fluid velocity in the Cartesian x direction (m.s^{-1})
s	Slip velocity (m.s^{-1})	$\vec{v}_{f,y}$	Fluid velocity in the Cartesian y direction (m.s^{-1})
τ_w	Wall shear stress	$\vec{v}_{p,x}$	Particle velocity in the Cartesian x direction (m.s^{-1})
u	Axial velocity (m.s^{-1})	$\vec{v}_{p,y}$	Particle velocity in the Cartesian y direction (m.s^{-1})
U_b	Bulk velocity (m.s^{-1})	v_p	Cuttings/particle velocity (m.s^{-1})
U_τ	Friction velocity at the nearest wall	w	Tangential velocity (m.s^{-1})
v	Local kinematic viscosity (m^2.s^{-1})		
v_{circ}	Fluid circulation velocity (m.s^{-1})		
XG	Xanthan Gum		
y	First layer thickness (m)		
y^+	Dimensionless wall distance		

Greek letters

α_p	Particle volume fraction (-)
α_f	Fluid phase volume fraction (-)
μ_p	Total particle viscosity (Pa.s)
μ_p	Fluid phase viscosity (Pa.s)
$\mu_{p,\,col}$	Collisional viscosity (Pa.s)
$\mu_{p,\,kin}$	Kinetic viscosity (Pa.s)
$\mu_{p,\,fr}$	Frictional viscosity (Pa.s)
λ_p	Particle bulk viscosity (Pa.s)
μ_f	Fluid viscosity (Pa.s)
Θ_p	Granular temperature (K)
ρ_p	Solid phase density (kg.m^{-3})
ρ_f	Fluid density (kg.m^{-3})
$\hat{\rho}_q$	Effective phase density (kg.m^{-3})
φ	Hole inclination angle (degrees)
δ	Offset distance (m)
ϕ	Angle of internal friction (degrees)
σ	Dimensionless annular space (-)
Ω	Angular velocity of rotation (RPM)
τ	Shear stress (N.m^{-2})
γ	Shear rate (s^{-1})

6. References

Ahn, H. 1989. *Experiments and analytical investigations of granular materials: shear flow and convective heat transfer* (Doctoral dissertation, California Institute of Technology).

Akhshik, S., Behzad, M., & Rajabi, M. 2016. CFD-DEM simulation of the hole cleaning process in a deviated well drilling: The effects of particle shape. *Particuology*, **25**, 72-82.

Barigou, M. 2004. Particle tracking in opaque mixing systems: an overview of the capabilities of PET and PEPT. *Chem. Eng. Res. Des.* **82**(9), 1258-1267.

Bertrand, F., Leclaire, L. A., & Levecque, G. 2005. DEM-based models for the mixing of granular materials. *Chem. Eng. Sci.* **60**(8), 2517-2531.

Bilgesu, H. I., Ali, M. W., Aminian, K., & Ameri, S., 2002. Computational Fluid Dynamics (CFD) as a tool to study cutting transport in wellbores. In *SPE Eastern Regional Meeting*. Society of Petroleum Engineers.

Bilgesu, H., Mishra, N., & Ameri, S., 2007. Understanding the effect of drilling parameters on hole cleaning in horizontal and deviated wellbores using computational fluid dynamics. *Eastern Regional Meeting*. Society of Petroleum Engineers.

Binder, J. L., & Hanratty, T. J., 1991. A diffusion model for droplet deposition in gas/liquid annular flow. *Int. J. Multiph. Flow.* **17**(1), 1-11.

Brennen, C. E. 2005. Fundamentals of multiphase flow. Cambridge university press.

Capo, J., Yu, M., Miska, S., & Takach, N., 2004. Cuttings transport with aqueous foam at intermediate inclined wells. *SPE/ICoTA Coiled Tubing Conference and Exhibition*. Society of Petroleum Engineers.

Cimbala, J. M., & Çengel, Y. A., 2014. Fluid mechanics: fundamentals and applications.

Chein, R., & Chung, J. N., 1987. Effects of vortex pairing on particle dispersion in turbulent shear flows. *Int. J. Multiph. Flow.* **13**(6), 785-802.

Chen, Z., Ahmed, R., Miska, S., & Takach, N., 2007. Experimental study on cuttings transport with foam under simulated horizontal downhole conditions. *SPE Drill. & Compl.* **22**(04), 304-312.

Crowe, C. T., Gore, R. A., & Troutt, T. R. (1985). Particle dispersion by coherent structures in free shear flows. *Part. Sci. Technol.* **3**(3-4), 149-158.

Crowe, C. T., Schwarzkopf, J. D., Sommerfeld, M., & Tsuji, Y., 2011. Multiphase flows with droplets and particles. CRC press.

Demiralp, Y., 2014. Effects Of Drill-pipe Whirling Motion on Cuttings Transport Performance for Horizontal Drilling. *Master dissertation*. Louisiana State University, USA.

Duan, M., Miska, S. Z., Yu, M., Takach, N. E., Ahmed, R. M., & Zettner, C. M., 2006. Transport of small cuttings in extended reach drilling. *International Oil & Gas Conference and Exhibition in China*. Society of Petroleum Engineers.

Duan, M., Miska, S. Z., Yu, M., Takach, N. E., Ahmed, R. M., & Hallman, J. H., 2008. The effect of drillpipe rotation on pressure losses and fluid velocity profile in foam drilling. In *SPE Western Regional and Pacific Section AAPG Joint Meeting*. Society of Petroleum Engineers.

Duan, M., Miska, S., Yu, M., & Takach, N., 2010. Experimental study and modeling of cuttings transport using foam with drill pipe rotation. *SPE Drill. & Compl.* **25**(03), 352-362.

Eesa, M., Barigou, M., 2008. Horizontal laminar flow of coarse nearly-neutrally buoyant particles in non-Newtonian conveying fluids: CFD and PEPT experiments compared. *Int. J. Multiph. Flow.* **34**(11), 997-1007.

Eesa, M., & Barigou, M., 2009. CFD investigation of the pipe transport of coarse solids in laminar power law fluids. *Chem. Eng. Sci.* **64**(2), 322-333.

Epelle, E. I., & Gerogiorgis, D. I. 2017. A multiparametric CFD analysis of multiphase annular flows for oil and gas drilling applications. *Comput. Chem. Eng.* 106, 645-661.

Escudier, M. P. P. J., Oliveira, P. J., Pinho, F., & Smith, S. (2002). Fully developed laminar flow of non-Newtonian liquids through annuli: comparison of numerical calculations with experiments. *Exp. Fluids*, **33**(1), 101-111.

Fluent, A. 2017. 18.0 ANSYS Fluent theory guide 18.0. *Ansys Inc*, U.S.A.

Fan, L. S., & Zhu, C. 2005. *Principles of gas-solid flows*. Cambridge University Press.

Garcia-Hernandez, A. J., Miska, S. Z., Yu, M., Takach, N. E., & Zettner, C. M., 2007. Determination of cuttings lag in horizontal and deviated wells. *SPE Annual Technical Conference and Exhibition*. Society of Petroleum Engineers.

Gidaspow, D., 1994. Multiphase flow and fluidization: continuum and kinetic theory descriptions. Academic press.

Hetsroni, G. 1989. Particles-turbulence interaction. *Int. J. Multiph. Flow.* **15**(5), 735-746.

Han, S., Hwang, Y., Woo, N., & Kim, Y., 2010. Solid–liquid hydrodynamics in a slim hole drilling annulus. *J. Pet. Sci. Eng.* **70**(3), 308-319.

Heydari, O., Sahraei, E., & Skalle, P., 2017. Investigating the impact of drillpipe's rotation and eccentricity on cuttings transport phenomenon in various horizontal annuluses using computational fluid dynamics (CFD). *J. Pet. Sci. Eng.* **156**, 801-813.

Johnson, P. C., & Jackson, R., 1987. Frictional–collisional constitutive relations for granular materials, with application to plane shearing. *J. Fluid Mech.* **176**, 67-93.

Kline, S. J., Reynolds, W. C., Schraub, F. A., & Runstadler, P. W., 1967. The structure of turbulent boundary layers. *J. Fluid Mech.* **30**(4), 741-773.

Larsen, T., Pilehvari, A., & Azar, J., 1997. Development of a new cuttings-transport model for high-angle wellbores including horizontal wells. *SPE Drill. & Compl.* **12**(02), 129-136.

Lien, K., Monty, J. P., Chong, M. S., & Ooi, A., 2004. The entrance length for fully developed turbulent channel flow. In *15th Aust. Fluid Mech. Conference*. **15**, 356-363.

Liu, Y., 2014. Two-fluid modeling of gas-solid and gas-liquid flows: solver development and application. *Doctoral dissertation*, Universitätsbibliothek der TU München.

Lun, C., Savage, S., & Jeffrey, D., 1984. Kinetic theories for granular flow: inelastic particles in Couette flow and slightly inelastic particles in a general flowfield. *J. Fluid Mech*. **140**, 223-256.

Mei, R., & Klausner, J., 1994. Shear lift force on spherical bubbles. *Int. J. Heat Fluid Flow* **15**(1), 62-65.

Mishra, N., 2007. Investigation of hole cleaning parameters using computational fluid dynamics in horizontal and deviated wells. *Master dissertation,* West Virginia University, USA.

Moraga, F., Bonetto, F., & Lahey, R., 1999. Lateral forces on spheres in turbulent uniform shear flow. *Int. J. Multiph. Flow*. **25**(6), 1321-1372.

Nikuradze, J. (1933). Regularities of the turbulent flow in smooth pipes (supplement). *Research in Engineering* , **4**(1), 44-44.

Nouri, J. M., & Whitelaw, J. H., 1994. Flow of Newtonian and non-Newtonian fluids in a concentric annulus with rotation of the inner cylinder. *Trans.-Am. Soc. Mech. Eng. J. Fluids Eng*. **116**, 821-821.

Nouri, J. M., & Whitelaw, J. H., 1997. Flow of Newtonian and non-Newtonian fluids in an eccentric annulus with rotation of the inner cylinder. *Int. J. Heat Fluid Flow*. **18**(2), 236-246.

Ofei, T., Irawan, S., & Pao, W., 2014. CFD method for predicting annular pressure losses and cuttings concentration in eccentric horizontal wells. *J. Pet. Eng.*

Osgouei, R., 2010. Determination of cuttings transport properties of gasified drilling fluids. *Doctoral dissertation*, Middle East Technical University, Turkey.

Ozbayoglu, M. E., Saasen, A., Sorgun, M., & Svanes, K., 2010. Critical fluid velocities for removing cuttings bed inside horizontal and deviated wells. *Pet. Sci. Technol*. **28**(6), 594-602.

Pereira, F. A. R., Ataíde, C. H., & Barrozo, M. A. S., 2010. CFD approach using a discrete phase model for annular flow analysis. *Latin Am. Appl. Res*. **40**(1), 53–60.

Roco, M. C. (Ed.)., 1993. *Particulate two-phase flow* (Vol. 1002). Boston, MA: Butterworth-Heinemann.

Roco, M. C., & Shook, C. A., 1983. Modeling of slurry flow: the effect of particle size. *Can. J. Chem. Eng*. **61**(4), 494–503.

Rooki, R., Ardejani, F., & Moradzadeh, A., 2015. CFD Simulation of Rheological Model Effect on Cuttings Transport. *J. Dispersion Sci. Tech*. **36**(3), 402-410.

Rooki, R., Doulati Ardejani, F., Moradzadeh, A., & Norouzi, M., 2014. Simulation of cuttings transport with foam in deviated wellbores using computational fluid dynamics. *J. Pet. Explor. Prod. Technol*. **4**(3), 263–273.

Saffman, P., 1965. The lift on a small sphere in a slow shear flow. *J.Fluid Mech*. **22**(02), 385-400.

Schaeffer, D., 1987. Instability in the evolution equations describing incompressible granular flow. *J. Diff. Eqns*. **66**(1), 19-50.

Sorgun, M., 2010. Modeling of Newtonian fluids and cuttings transport analysis in high inclination wellbores with pipe rotation. *Doctoral Dissertation*. Middle East Technical Univeristy, Turkey.

Subramaniam, S., 2013. Lagrangian–Eulerian methods for multiphase flows. *Prog. Energy Combust. Sci*. **39**(2), 215-245.

Tang, L. F. Y. C. T. J. N. T. R., Wen, F., Yang, Y., Crowe, C. T., Chung, J. N., & Troutt, T. R., 1992. Self-organizing particle dispersion mechanism in a plane wake. *Physics of Fluids A: Fluid Dynamics*, **4**(10), 2244-2251.

Tomren, P., Iyoho, A., & Azar, J., 1986. Experimental study of cuttings transport in directional wells. *SPE Drill. Eng*. **1**(01), 43-56.

Wang, Z., Guo, X., Ming, L., & Hong, Y., 2009. Effect of drill pipe rotation on borehole cleaning for extended reach well. *J. Hydrodyn. Ser. B.* **21**(3), 366-372.

Wen, C. Y., & Yu, Y. H., 1966. Mechanics of fluidization. *Chem. Eng. Prog. Symp. Ser.* **62**(1), 100–111.

Yilmaz, D., 2012. Discrete Phase Simulations of Drilled Cuttings Transport Process in Highly Deviated Wells. *Master dissertation*, Louisiana State University, USA.

Xu, J., Ozbayoglu, E., Miska, S. Z., Yu, M., & Takach, N., 2013. Cuttings Transport with Foam in Highly Inclined Wells at Simulated Downhole Conditions/Transport urobku wiertniczego przy użyciu piany w silnie nachylonych otworach w symulowanych warunkach w otworze. *Archives of Mining Sciences*, **58**(2), 481-494.

7. Appendix
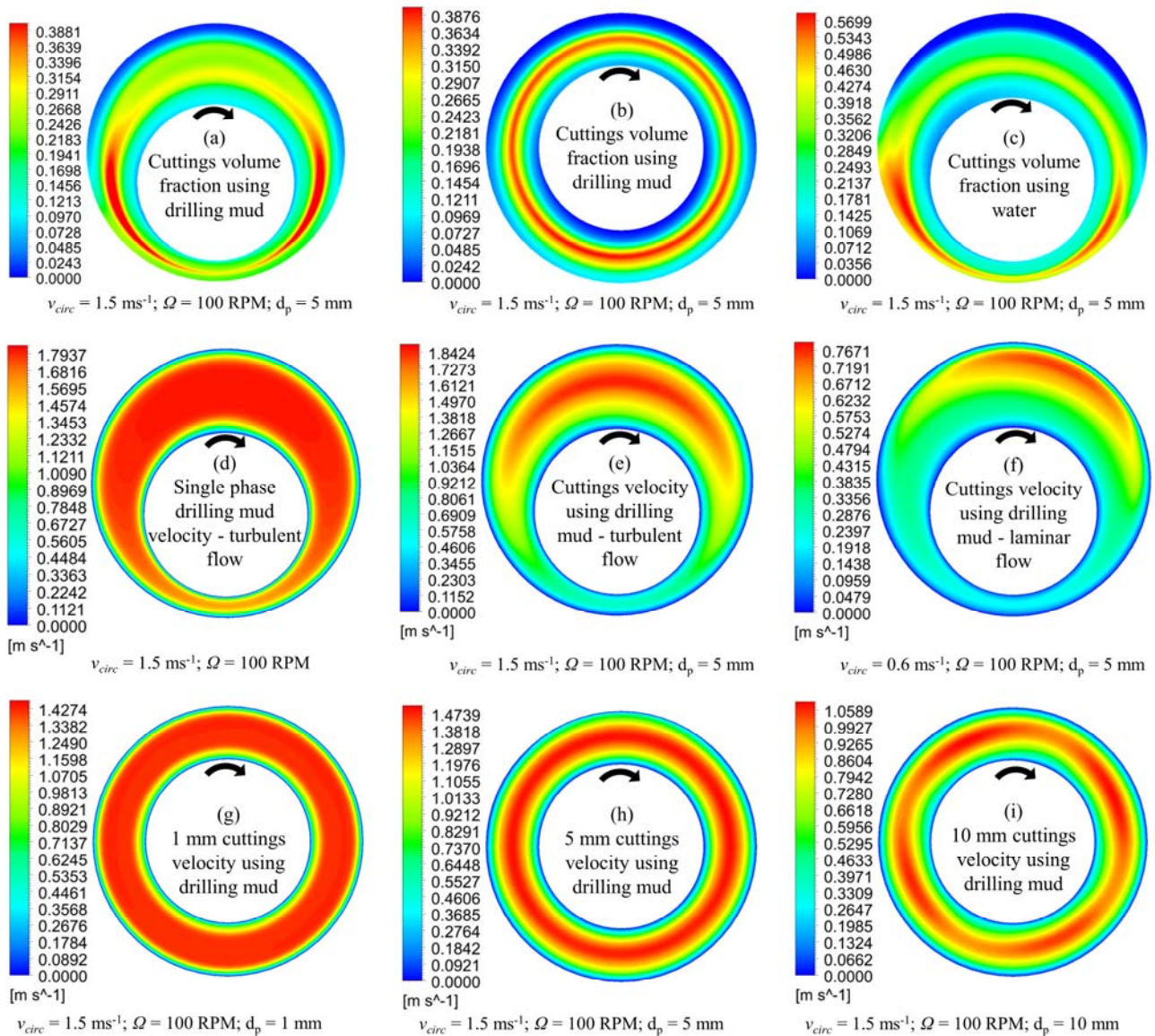
A - Contour plots (EE model)

Fig. 21. Contour plots of volume fraction and velocities of drill cuttings and fluid at different flow conditions.
Fig. 21 (a) shows increased concentration on the sides of the annulus; however the concentric case (b) has an even distribution of cuttings in the central region. Increased deposition is noticed with water as the carrier fluid (c). Previous work with a drilling mud of higher quality (Epelle and Gerogiorgis, 2017) showed even cuttings velocity profiles; however, the cuttings distribution observed here exhibit a strong spatial variation around the annulus. Fig. 21(d) shows the high fluid velocity obtainable in single phase flow; this is dampened by the introduction of cuttings (e) and (f). The impact of drillpipe rotation on the asymmetric velocity distribution is stronger under laminar conditions; this is not noticed in (e). Areas of high cuttings velocity around the annulus (an indication of particle dispersion) decreases with the increase in cuttings diameter as seen in (g), (h) and (i) respectively.

B - Particle flow behaviour (LE model)

Turbulent flow regime

(a) 1 second

(b) 2 seconds

(c) 3 seconds

Laminar flow regime
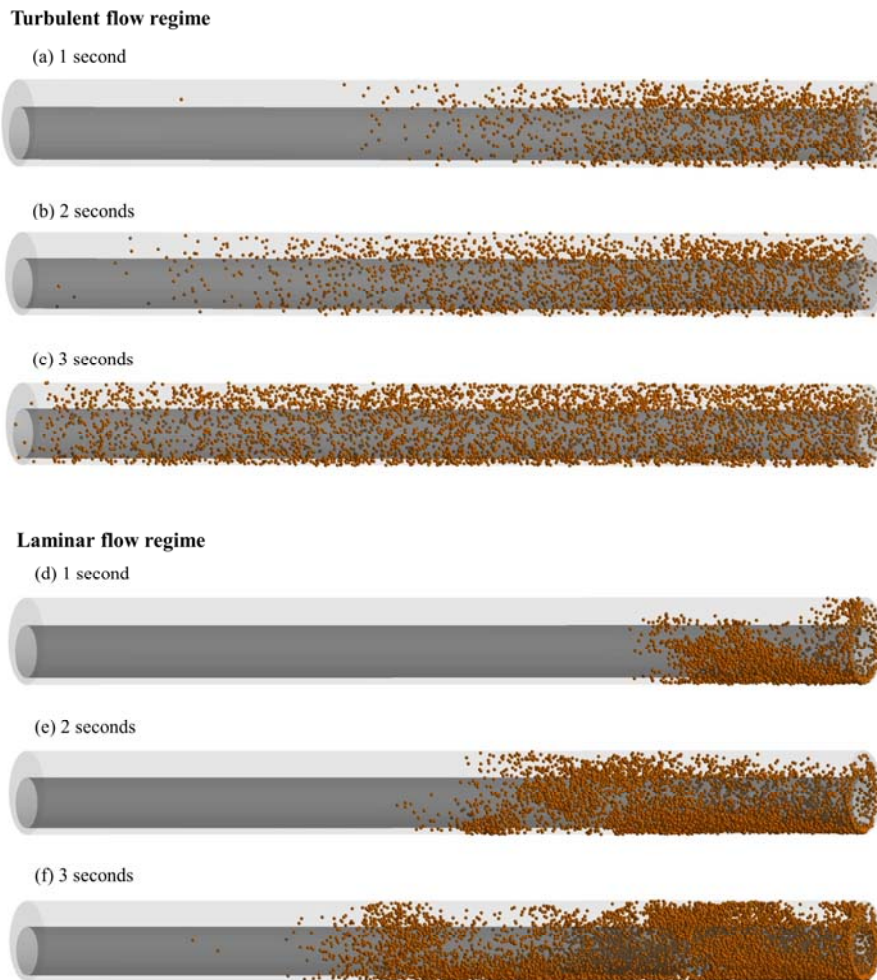
(d) 1 second

(e) 2 seconds

(f) 3 seconds

Fig. 22. Snapshots of particle (5 mm) flow behaviour in turbulent (a-c) and laminar (d-f) flow regimes.

In order to qualitatively understand the impact of turbulence ($v_{circ} = 2$ ms^{-1}) on cuttings transport, laminar flow conditions ($v_{circ} = 0.6$ ms^{-1}) were also simulated. With increased flow time, particles gradually fill up the annulus in a uniform manner under turbulent conditions. In the laminar flow regime, inter-particle spacing is low, thus yielding slight cuttings deposition. Drillpipe rotation (100 RPM) is seen to lift and sway particles as the flow progresses and this aids the transport process. In order to attain a statistically steady state (in which particles fully traverse the annular length) at laminar conditions, the simulation has to be run for longer periods.